

Anticancer Properties of an Important Drug Lead Podophyllotoxin Can Be Efficiently Mimicked by Diverse Heterocyclic Scaffolds Accessible via One-Step Synthesis

Igor V. Magedov,^{*,†} Liliya Frolova,[†] Madhuri Manpadi,[†] Uma devi Bhoga,[§] Hong Tang,[‡] Nikolai M. Evdokimov,[†] Olivia George,^{||} Kathy Hadje Georgiou,[§] Steffen Renner,[⊥] Matthäus Getlik,[#] Tiffany L. Kinnibrugh,[†] Manuel A. Fernandes,[§] Severine Van slambrouck,[†] Wim F. A. Steelant,^{†,●} Charles B. Shuster,^{||} Snezna Rogelj,[‡] Willem A. L. van Otterlo,^{*,§,∞} and Alexander Kornienko^{*,†}

[†]Department of Chemistry, and [‡]Department of Biology, New Mexico Institute of Mining and Technology, Socorro, New Mexico 87801, United States

[§]Molecular Sciences Institute, School of Chemistry, University of the Witwatersrand, PO Wits, 2050 Johannesburg, South Africa

^{||}Department of Biology, New Mexico State University, Las Cruces, New Mexico 88003, United States

[⊥]Max Planck Institute for Molecular Physiology, Dortmund, Germany

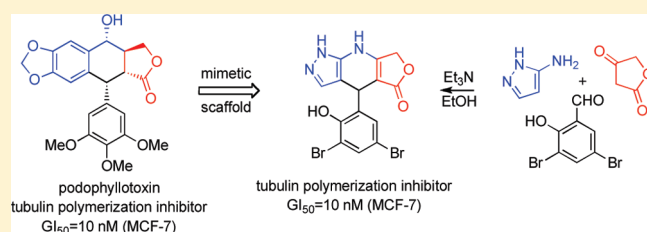
[#]Chemical Genomics Centre of the Max Planck Society, Dortmund, Germany

[∞]Department of Chemistry and Polymer Sciences, Stellenbosch University, Stellenbosch 7600, Western Cape, South Africa

S Supporting Information

ABSTRACT: Structural simplification of an antimitotic natural product podophyllotoxin with mimetic heterocyclic scaffolds constructed using multicomponent reactions led to the identification of compounds exhibiting low nanomolar antiproliferative and apoptosis-inducing properties. The most potent compounds were found in the dihydropyridopyrazole, dihydropyridonaphthalene, dihydropyridoindole, and dihydropyridopyrimidine scaffold series. Biochemical mechanistic studies performed with dihydropyridopyrazole compounds showed

that these heterocycles inhibit *in vitro* tubulin polymerization and disrupt the formation of mitotic spindles in dividing cells at low nanomolar concentrations, in a manner similar to podophyllotoxin itself. Separation of a racemic dihydropyridonaphthalene into individual enantiomers demonstrated that only the optical antipode matching the absolute configuration of podophyllotoxin possessed potent anticancer activity. Computer modeling, performed using the podophyllotoxin binding site on β -tubulin, provided a theoretical understanding of these successful experimental findings.



INTRODUCTION

Natural products are often referred to as evolutionarily selected “privileged structures” that are likely to manifest multiple biological activities.¹ Because of their intrinsic biorelevance, they have historically been a major source of new pharmaceuticals. For example, in the area of cancer, the fraction of drugs derived from natural products amounts to 60% and hit rates obtained by screening of natural product-derived collections of compounds are dramatically higher than those resulting from high throughput screens of combinatorial libraries.^{2,3} However, the structures of natural products are generally quite complex, incorporating intricate ring systems and large numbers of stereogenic centers. Therefore, preparations of natural-product-based libraries inevitably involve rather sophisticated and laborious synthetic sequences. Furthermore, therapeutic development of promising leads resulting from these libraries is significantly impeded by the problem of large-scale compound

supply. These challenges are becoming increasingly more relevant because of the renewed interest in natural products by the pharmaceutical industry and the failure of alternative methods to deliver many therapeutic lead compounds.⁴

In a search for general solutions to the above-mentioned problems, we have initiated a research program aimed at structural simplification of bioactive natural products by designing mimetic scaffolds that can be constructed using one-step multicomponent reactions (MCRs).⁵ We recently described a dihydropyridopyrazole scaffold designed on the basis of a potent anticancer cyclolignan, podophyllotoxin, and readily prepared by combining an aminopyrazole, tetronic acid, and an aromatic or heteroaromatic aldehyde in a one-pot condensation process (Figure 1).^{5a,b}

Received: April 6, 2011

Published: May 26, 2011

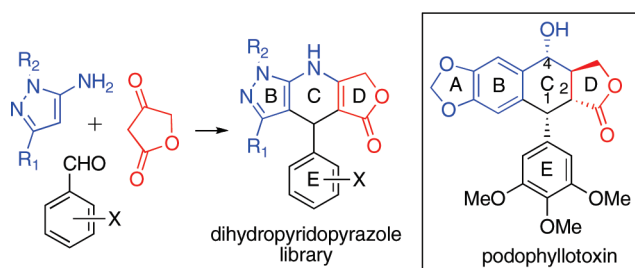


Figure 1. Podophyllotoxin-mimetic dihydropyridopyrazole library.

The utilization of podophyllotoxin as a lead in anticancer drug design has resulted in useful cancer fighting drugs such as etoposide, teniposide, and etoposide phosphate.⁶ These successes have fueled further research efforts in this area directed at the preparation of analogues, which are expected to have improved potency and reduced toxicity. Unfortunately, the complex chemical structure of podophyllotoxin virtually prevents the generation of its analogues from simple commercially available materials, and therefore, derivatization of podophyllotoxin has been the main strategy to obtain structure–activity relationship (SAR) information.⁷ This SAR has often not been systematic and has been limited by the type of chemistry that podophyllotoxin can undergo. As a result many designed analogues are synthetically inaccessible from the parent natural product. For example, modifications of ring E are extremely difficult because of the presence of the three methoxy groups in the starting lignan. To achieve useful modifications of ring E, one therefore needs to resort to total synthesis efforts. Indeed, Berkowitz and co-workers achieved a total synthesis of the 3',4',5'-tridemethoxy analogue of podophyllotoxin (ring E = Ph), which is inaccessible by derivatization of the natural product itself.⁸ However, the length of the synthetic route, which involved 19 steps from commercially available materials, serves to illustrate the challenge a medicinal chemist would face following such a strategy. The versatility of the MCR approach, however, has allowed us to prepare a diverse library of podophyllotoxin mimetics and generate systematic SAR data. Thus, the utilization of requisite aldehyde starting materials leads directly to the desired modification of ring E (Figure 1). Furthermore, the use of various aromatic and heteroaromatic amines in lieu of the aminopyrazole component has allowed us to expand the scope of possible A,B-ring system substitutions in these podophyllotoxin-mimetic scaffolds. Such SAR-guided structure optimization work and biochemical mechanistic investigations have led to several important breakthroughs in this area of research. First, we were able to significantly enhance the potency and identify compounds that rival podophyllotoxin in antiproliferative and apoptosis-inducing properties. Second, we obtained strong evidence that the dihydropyridopyrazoles retain the anti-tubulin mode of action of the natural cyclolignan, attesting to the bona fide mimicry of the podophyllotoxin's structure by this heterocyclic scaffold. Third, we found that nanomolar antiproliferative potencies are not limited to compounds based on the dihydropyridopyrazole scaffold but also reside with dihydropyridonaphthalene, dihydropyridindole, and dihydropyridopyrimidine mimetic libraries, pointing to the possibility of scaffold modification as an additional option in the pursuit of a tubulin-targeting clinically useful anticancer agent. Finally, computational studies revealed a structural basis for these successful findings and further supported the theoretical framework of the approach. Altogether, the results

Table 1. Synthesis and Antiproliferative Activity of Dihydropyridopyrazoles

#	Ar	R	%	GI ₅₀ (μM) ^[a]	
				HeLa	MCF-7
1		Me	80	5.0 ± 0.5	5.0 ± 0.5
2		H	75	3.0 ± 0.1	0.25 ± 0.06
3		Me	78	0.75 ± 0.10	1.0 ± 0.1
4		H	72	0.75 ± 0.05	0.25 ± 0.06
5		Me	76	3.0 ± 0.1	4.0 ± 0.3
6		H	71	0.075 ± 0.005	0.10 ± 0.01
7		Me	88	3.0 ± 0.5	0.8 ± 0.1
8		H	76	0.075 ± 0.015	0.015 ± 0.010
9		Me	85	0.075 ± 0.010	0.075 ± 0.006
10		H	83	0.025 ± 0.008	0.025 ± 0.003
11		Me	85	0.035 ± 0.004	0.10 ± 0.04
12		H	81	0.025 ± 0.003	0.030 ± 0.005
13		Me	83	0.30 ± 0.08	0.25 ± 0.05
14		H	74	0.050 ± 0.005	0.025 ± 0.004
15		H	70	2.0 ± 0.3	0.50 ± 0.07
16		H	76	0.020 ± 0.005	0.010 ± 0.003
17		H	10	1.15 ± 0.05	0.74 ± 0.04
	Podophyllotoxin			0.020 ± 0.002	0.010 ± 0.003

^a Concentration required to reduce the viability of cells by 50%, after 48 h of treatment with indicated compounds, relative to DMSO control, ±SD from two independent experiments, each performed in eight replicates, determined by MTT assay.

of this study present a strong case for establishing the mimetic scaffold approach as a useful paradigm in drug discovery.

RESULTS AND DISCUSSION

Optimized Dihydropyridopyrazoles Rival Podophyllotoxin in Antiproliferative Effect. Because the A,B-ring system in podophyllotoxin is sterically more demanding and less polar than the pyrazole ring, we initially expected that some degree of substitution of the pyrazole moiety would be required for activity and focused on the C-3 Me-substituted compounds (R¹ = Me, R² = H, Figure 1).^{5a,b} Further work revealed, however, that low nanomolar potencies are predominantly associated with compounds containing the unsubstituted pyrazole moiety (R = H, Table 1). Synthesis of such compounds involved combining 5-aminopyrazole, tetronic acid, and an aromatic aldehyde in ethanol and refluxing these reaction mixtures for 0.5–3 h. The desired dihydropyridopyrazoles precipitated upon cooling to

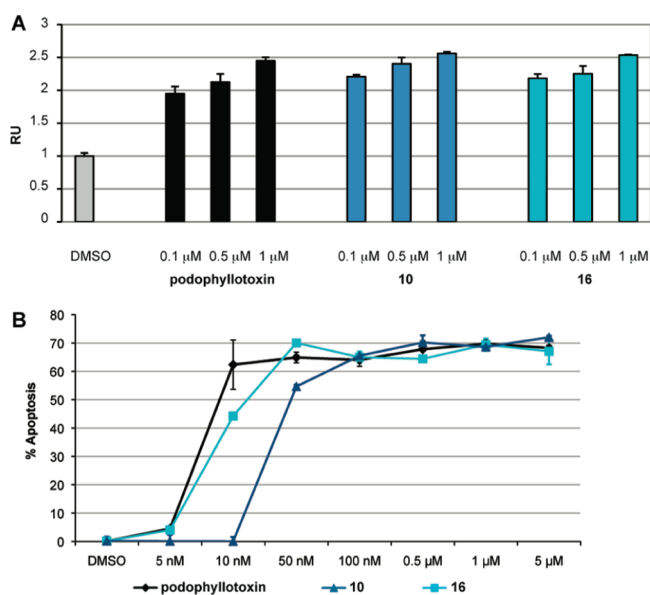


Figure 2. (A) Caspase-3 activation in Jurkat cells with indicated compounds. The magnitudes of activation are expressed as relative units (RU) with DMSO control assigned the value of 1. Error bars represent data from two independent experiments, each performed in quadruplicate. (B) Percent apoptotic cells after 48 h of treatment with indicated compounds \pm SD from two independent experiments, each performed in three replicates, determined by flow cytometric annexin-V/propidium iodide assay.

room temperature. In addition, in most cases the products were analytically pure without any further purification. Evaluation of these heterocycles for antiproliferative activity was performed using HeLa and MCF-7 cancer cell lines as models for human cervical and breast adenocarcinomas, respectively (Table 1). While the structural requirements of ring E in podophyllotoxin have seen little investigation (because of the synthetically unsurmountable challenge of removing or replacing the methoxy groups), our data show that in the dihydropyridopyrazole series the methoxy substituents are not important and the combination of 3-bromo with 2-hydroxy substitution brings about the highest potencies. Thus, the progressive replacement of the methoxy groups with meta-bromo substitution (2 \rightarrow 4 \rightarrow 6 \rightarrow 10) and the subsequent addition of a 2-hydroxy group (12, 14, and 16) led to compounds with low nanomolar potencies. Of particular note was that the 3,5-dibromo-2-hydroxy compound (16) is equipotent to podophyllotoxin with GI_{50} values of 20 and 10 nM against HeLa and MCF-7 cells, respectively.

Optimized Dihydropyridopyrazoles Rival Podophyllotoxin in Apoptosis-Inducing Effect. Because the anticancer efficacy of many current chemotherapeutic agents is strongly correlated with their ability to induce apoptosis in cancer cells,⁹ we compared the apoptosis-inducing potential of the potent dihydropyridopyrazoles with that of podophyllotoxin. This was accomplished by performing caspase-3 activation¹⁰ and flow cytometric annexin-V/propidium iodide¹¹ assays, two common methods used to detect and quantify such hallmarks of the apoptotic process as caspase cascade activation and the appearance of the phosphatidylserine lipid in the outer leaflet of the cellular membrane (Figure 2). These assays, carried out with Jurkat cells (a model for T-cell leukemia), revealed that both podophyllotoxin and the 3,5-dibromo analogues 10 and 16

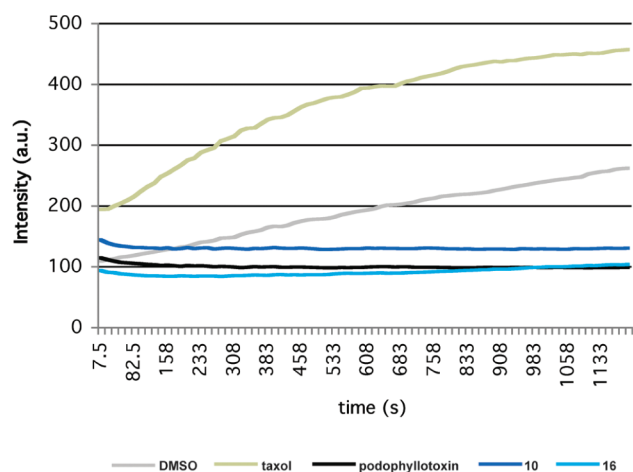


Figure 3. Effect of dihydropyridopyrazoles on tubulin polymerization in vitro. Paclitaxel (3 μ M) promotes microtubule formation relative to 0.05% DMSO control. In contrast, 10 (25 μ M), 16 (25 μ M), and podophyllotoxin (25 μ M) completely suppress tubulin polymerization.

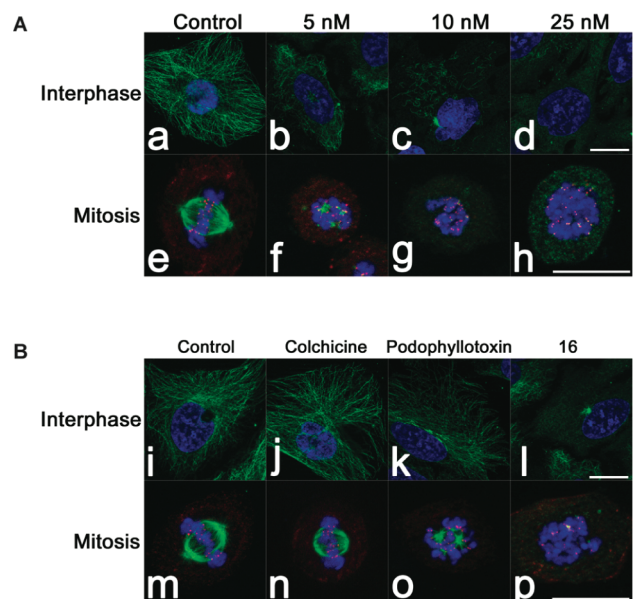


Figure 4. Microtubule organization in interphase and mitotic HeLa cells treated with (A) 16 at the indicated concentrations and (B) indicated agents at 5 nM: microtubules (green), the kinetochore marker Hec1 (red, panels e–h and m–p), and Hoechst 33342 (blue). Scale bars, 10 μ m.

exhibit similar magnitudes of apoptosis induction at high nanomolar concentrations (Figure 2A). In addition, similar to podophyllotoxin, the induction of apoptosis by 16 occurs at concentrations as low as 5–8 nM (Figure 2B), an observation that is consistent with the beneficial effect of the 2-hydroxy substituent in combination with the 3,5-dibromo substitution in ring E.

Dihydropyridopyrazoles Retain Anti-Tubulin Mode of Action of Podophyllotoxin. Using flow cytometric cell cycle analysis, we obtained evidence pointing to the retention of the anti-tubulin mechanism of action by the dihydropyridopyrazoles. Agents interfering with tubulin dynamics are known to arrest cells in M phase of the cell cycle.¹² Thus, similar to that of

antimitotic podophyllotoxin, these compounds cause the accumulation of Jurkat cell populations with a 4N DNA content (data not shown). To confirm the retention of microtubule-destabilizing activity *in vitro*, a fluorimetry-based microtubule polymerization assay was employed.¹³ While paclitaxel exhibited enhancement of microtubule formation relative to the effect of the DMSO control (Figure 3), library members **10** and **16** displayed a potent microtubule destabilizing effect in a manner similar to the tubulin polymerization inhibitor podophyllotoxin.

Similarly, examination of cultured HeLa cervical human cells treated with the dihydropyridopyrazoles revealed potent microtubule destabilizing activities. Analogue **16** disrupted both interphase and mitotic microtubule organization at concentrations as low as 5 nM. As shown in Figure 4A (panel f), microtubules nucleating from the spindle poles are visible, but at 10 nM (panel g), virtually all microtubule nucleation from either spindle poles or kinetochores is ablated. In comparison, colchicine displayed no visible defect in microtubule organization at 5 nM (Figure 4B, panels j and n), whereas positive control podophyllotoxin caused

similar effects on mitotic spindle formation (panel o) with no effect on interphase microtubule organization (panel k).

Further Scaffold Modifications Lead to Compounds Possessing Single-Digit Nanomolar Antiproliferative Potencies.

In an attempt to expand the range of possible A,B-ring system substitutions in these podophyllotoxin-mimetic scaffolds, we explored the use of various aromatic and heteroaromatic amines in lieu of the aminopyrazole component in the MCR process. The MCR literature contains a number of examples of cyclocondensation of aromatic amines with aldehydes and 1,3-dicarbonyl compounds.¹⁴ Importantly, as this work was in progress, scientists at Bayer CropScience AG utilized diversely substituted anilines in this process and prepared over 140 such heterologans for their potential use as anti-insecticidal agents.^{14a} Furthermore, an MCR involving naphthylamines, 1,3-dicarbonyl compounds, and aldehydes had also been previously investigated by other researchers.¹⁵ Prompted by these successful literature examples, as well as by the results of computational docking studies (*vide infra*) that indicated that large hydrophobic residues in lieu of the A,B-ring system in podophyllotoxin could be accommodated at the binding site on β -tubulin, we investigated the reaction of α -naphthylamine with tetrone acid and diversely substituted benzaldehydes (Figure 5, Table 2). The MCR was found to be as practical as that involving aminopyrazoles and the desired pentacycles precipitated from the refluxing ethanol solutions. However, the reaction yields were somewhat eroded, possibly by a number of competing side reactions. Thus, the desired pentacycle **B** can further react with the Knoevenagel intermediate **A** at the second nucleophilic position of the nitrogen-bearing aromatic ring to give side product **C** (Figure 5), an outcome consistent with the experimental findings of Frackenpohl *et al.*^{14a} In addition, further slight reduction in reaction yields was observed in the case of 7-hydroxy- α -naphthylamine. It is likely that the presence of the naphtholic hydroxyl leads to side products **D**, as naphthols have been shown to be substrates for such MCR processes.¹⁶

The evaluation of these compounds for antiproliferative activity against HeLa and MCF-7 cells indicated that they are more potent than podophyllotoxin itself, and many of them have GI₅₀ values as low as 3 nM (Table 2). The addition of a hydroxyl group to the naphtholic moiety had a beneficial effect by further lowering the GI₅₀ values, which is an excellent finding considering the

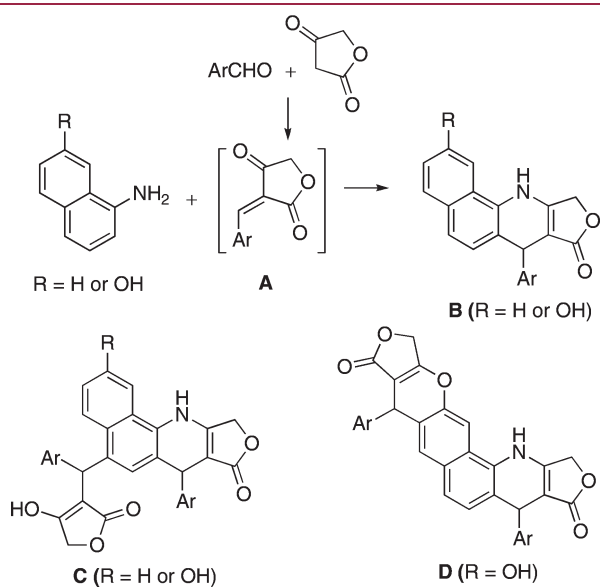


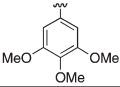
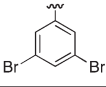
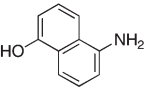
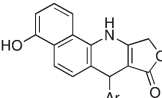
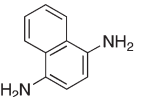
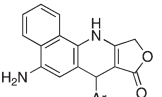
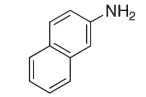
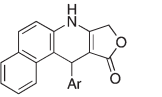
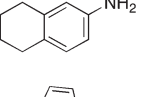
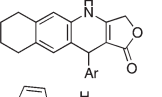
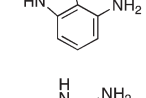
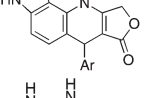
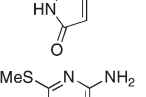
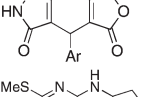
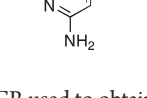
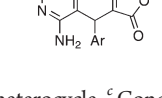
Figure 5. MCR utilizing α -naphthylamines and possible side products.

Table 2. Synthetic Yields and Antiproliferative Activity (nM) of α -Naphthylamine-Based Podophyllotoxin-Mimetics

MCR product	Ar	MeO	Br	Br	Br	Br	Br	Br	Br	S
	18 : ^a 14% ^b	19 : 39%	20 : 22%	21 : 41%	22 : 74%	23 : 68%	24 : 35%	25 : 56%		
	3 \pm 0 ^c	16 \pm 2	3 \pm 0	18 \pm 2	3 \pm 0	3 \pm 0	7 \pm 2	3 \pm 0		
	3 \pm 0 ^d	14 \pm 1	3 \pm 0	21 \pm 1	3 \pm 0	3 \pm 0	13 \pm 3	3 \pm 0		
	26 : 63%	27 : 50%	28 : 34%	29 : 42%	30 : 58%	31 : 42%	32 : 28%	33 : 33%		
	2 \pm 0	6 \pm 1	2 \pm 0	7 \pm 4	6 \pm 1	3 \pm 1	3 \pm 0	3 \pm 0		
	3 \pm 1	3 \pm 0	3 \pm 0	3 \pm 0	3 \pm 0	3 \pm 1	3 \pm 0	3 \pm 0		

^a Compound number. ^b Synthetic yield of the MCR used to obtain this heterocycle. ^c Concentration (nM) required to reduce the viability of HeLa cells by 50% after 48 h of treatment with indicated compounds, relative to DMSO control; \pm SD from two independent experiments, each performed in eight replicates, determined by MTT assay. ^d Concentration (nM) required to reduce the viability of MCF-7 cells by 50% after 48 h of treatment with indicated compounds, relative to DMSO control; \pm SD from two independent experiments, each performed in eight replicates, determined by MTT assay.

Table 3. Further Exploration of A,B-Ring System Substitutions in Podophyllotoxin Mimetics

entry	starting amine	MCR product		synthetic yield and antiproliferative GI ₅₀ (nM)	
		Ar			
1			34 ^a : 59% ^b 3 ± 0 ^c 3 ± 0 ^d	35 : 77% 21 ± 2 23 ± 6	
2			36 : 0%	37 : 66% 21 ± 0 16 ± 4	
3			38 : 62% 540 ± 23 121 ± 3	39 : 78% 420 ± 180 201 ± 22	
4			40 : 13% 18 ± 1 19 ± 1	41 : 31% 100 ± 5 70 ± 54	
5			42 : 56% 19 ± 2 22 ± 1	43 : 39% 114 ± 0 21 ± 0	
6			44 : 45% >10,000 >10,000	45 : 38% >10,000 >10,000	
7			46 : 60% 125 ± 20 170 ± 25	47 : 36% 561 ± 290 1,020 ± 230	

^a Compound number. ^b Synthetic yield of the MCR used to obtain this heterocycle. ^c Concentration (nM) required to reduce the viability of HeLa cells by 50% after 48 h of treatment with indicated compounds, relative to DMSO control; ±SD from two independent experiments, each performed in eight replicates, determined by MTT assay. ^d Concentration (nM) required to reduce the viability of MCF-7 cells by 50% after 48 h of treatment with indicated compounds, relative to DMSO control; ±SD from two independent experiments, each performed in eight replicates, determined by MTT assay.

potential water solubility problems associated with these hydrophobic compounds.

Interestingly, the benefit of the 3-bromo substitution pattern in ring E, which was important in the case of the pyrazole-based scaffold (vide supra, Table 1), is absent in these naphthalene-fused pentacycles. In fact, the low nanomolar potencies were found for all 3-bromo-substituted ring E containing compounds (19–25 and 27–33), as well as the 3,4,5-trimethoxy-substituted ones (18 and 26). Therefore, in our further A,B-ring system modification efforts we limited the variations in the ring E moiety to just two, namely, the 3,4,5-trimethoxy and 3,5-dibromo substitution patterns (Table 3).

Repositioning of the hydroxyl group in the starting α -naphthylamine from C-7 to C-9 (Table 3, entry 1) did not affect the successful outcome of the MCR process, which produced pentacycles 34 and 35. Both compounds were found to have excellent antiproliferative potencies. However, the utilization of electron-rich naphthalene-1,4-diamine (entry 2) resulted in MCR products susceptible to aerial oxidation. While pentacycle 37 was synthesized in respectable yield and found to have excellent antiproliferative properties, compound 36 was too unstable for its chemical characterization and biological testing. Interestingly, the use of β -naphthylamine (entry 3) in the MCR process yields compounds 38 and 39, in which the polycyclic

scaffold is bent in the opposite direction compared with analogues 18–37. As would be expected, the electrophilic attack by the Knoevenagel intermediate occurs preferentially at the α position of the naphthalene system. In contrast, in the tetrahydro system (entry 4), where the steric factors become more important than the electronic ones, the electrophilic attack occurs at the β' position and linear polycycles 40 and 41 are obtained exclusively. These regiochemical assignments are consistent with the NMR data and confirmed by X-ray structure determinations of select analogues.¹⁷ The biological testing of analogues 38–41 revealed that such a change in topology of the polycyclic scaffold has a strong effect on the antiproliferative potencies, raising the GI₅₀ values by about 2 orders of magnitude (compare 18 and 38 in Tables 2 and 3). Lastly, the previously unknown MCR processes utilizing heterocyclic amines, such as aminoindole, aminopyrazolone, and aminopyrimidine, were performed and polycycles 42–47 were obtained in respectable yields (entries 5–7). Of these, the indole- and pyrimidine-containing analogues 42, 43 and 46, 47 exhibited nanomolar antiproliferative potencies. Overall, these experiments argue convincingly that nanomolar antiproliferative potencies can be achieved with a judicious choice of an A,B-ring system in the podophyllotoxin-mimetic libraries and highlight the scaffold modification as an additional resource in the pursuit of a tubulin-targeting clinically useful anticancer agent.

Ring E in Podophyllotoxin Mimetics Is Positioned Quasi-axially with Respect to the Rest of the Heterocyclic Scaffold. To gain insight into the possible causes of the efficient mimicry of podophyllotoxin by these heterocyclic compounds, we performed density functional theory (DFT) conformational optimizations using the dihydropyridopyrazole scaffold. It is well-established that the quasi-axial positioning of ring E with respect to the rest of the molecule (rings A, B, C, and D) of podophyllotoxin is a key requirement for both efficient binding to the colchicine site on β -tubulin and the resulting antimitotic activity in this series of compounds.^{7a} For example, dehydropodophyllotoxin containing the aromatic ring C is totally inactive, while picropodophyllin, epimeric at C-2 (see Figure 1 for position numbering) and containing the cis-lactone moiety, has a significantly diminished activity. Both of these substances lack the axial orientation of ring E.¹⁸ Our computational results reveal that the dihedral angle of ring E with respect to the ABCD ring system in dihydropyridopyrazole **1** (124° , Figure 6B) is close to that of deoxypodophyllotoxin (116° , Figure 6A), confirming the

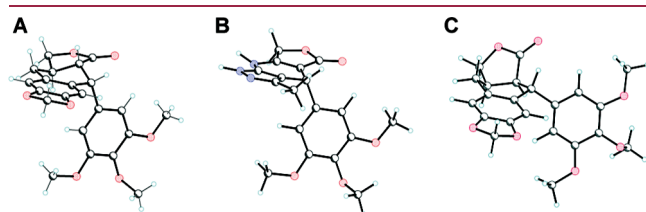


Figure 6. DFT optimizations of molecular geometries of (A) 4-deoxypodophyllotoxin, (B) dihydropyridopyrazole **1**, and (C) 4-deoxypicropodophyllin.

quasi-axial positioning of ring E in the dihydropyridopyrazole scaffold. In contrast, in deoxypicropodophyllin, ring E occupies an equatorial position (144° , Figure 6C).

Potent MCR Library Members Dock Well to the Podophyllotoxin Binding Site on β -Tubulin. On the basis of our design hypothesis, the novel tubulin inhibitors were assumed to have comparable binding modes in the tubulin colchicine binding site when compared to the design template podophyllotoxin. Computational docking simulations were thus used to further investigate the validity of our design hypothesis. Several of the synthesized molecules were docked into the tubulin–podophyllotoxin crystal structure from Knossow and co-workers¹⁹ (PDB code 1SA1). Despite a fairly low resolution of 4.2 Å and the absence of well-defined hydrogen bonds between podophyllotoxin and tubulin in the crystal structure, we were able to reproduce the observed binding mode of podophyllotoxin with good accuracy (rmsd = 0.936), as has also been reported by other groups.^{20,21}

Two major observations were made in the docking results. First, docking of the *R*-enantiomers of the compounds resulted in a comparable binding mode relative to podophyllotoxin, whereas the *S*-enantiomers led to an alternative binding mode with the ring systems flipped by 180° (vide infra). Second, we found that the most potent compounds, having additional rings added in a nonlinear bent arrangement relative to podophyllotoxin (e.g., **18–33**), were predicted to bind in a slightly twisted conformation, maximizing the overlap of the ring systems of our inhibitors with the ring system of podophyllotoxin (see the binding mode of *R*-**19** in Figure 7A). More interesting, this twisted orientation of the rings was still maintained in the tricycles that did not have additional rings and that did not have additional methyl groups on the B ring (see *R*-**16** in Figure 7B). If the methyl was present, a

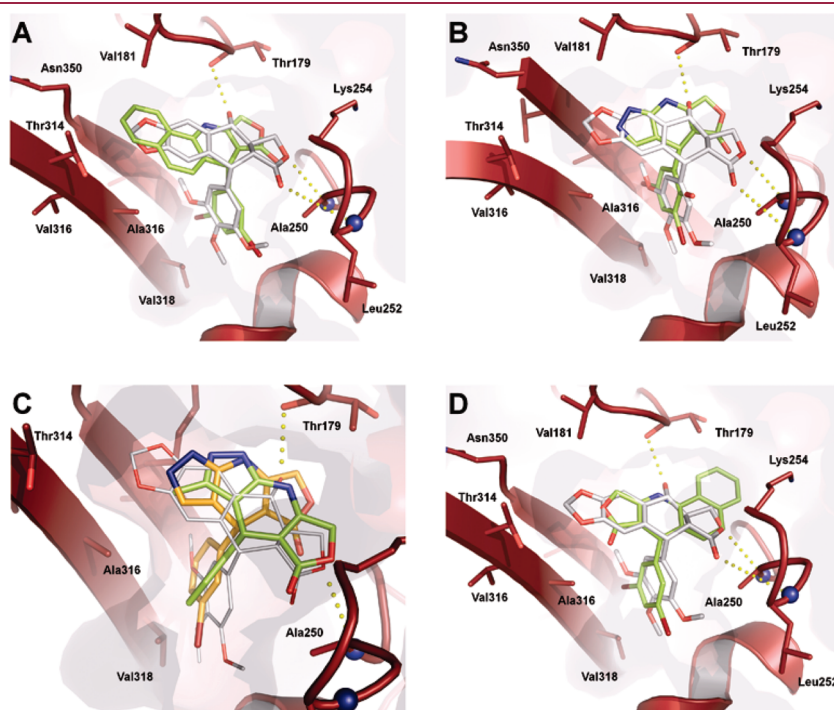


Figure 7. Representations of molecular dockings performed in this study, with all molecules overlaid with podophyllotoxin (in white): (a) *R*-**19**, representative of the binding mode of the most potent inhibitors with four ring-annulated systems; (b) *R*-**16**, representative of smaller, highly potent compounds with three ring annulated systems, binding analogous to *R*-**19**; (c) *R*-**5** (green) and *R*-**6** (orange). Compared to *R*-**6**, *R*-**5** has an additional methyl at the B ring that is responsible for a drop in potency and a twist away from the optimal binding mode [as in (a) and (b)] according to the docking study. (d) *S*-**19**, the less potent *S*-enantiomer of *R*-**19** binds in a “flipped” confirmation, relative to *R*-**19**.

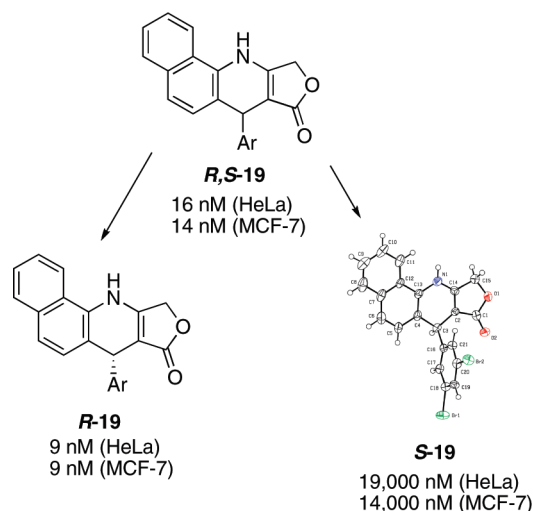


Figure 8. GI_{50} values of *R,S*-19, *R*-19, and *S*-19 toward HeLa and MCF-7 cell lines and X-ray structure of *S*-19 (note that only one of two molecules in the unit cell is shown and that the ORTEP diagram is shown at the 50% probability level).

different binding mode with a twist into the opposite direction (compared to podophyllotoxin) was observed (see *R*-5 in Figure 7C). This may explain the observed weakening effect of the B ring methyl group on the biological potency, for example, as found with pyrazoles *R*-5 and *R*-6, the former only differing by the extra methyl group but being significantly less potent than *R*-6. According to the docking study the additional methyl would clash with the protein and prevent the preferred binding mode. Other ligands with groups protruding into the same direction, like 38 and 39, which have an additional ring occupying the same space as the pyrazole methyl group, and compounds 44, 45, having a carbonyl group pointing into this direction, were also found to be significantly less potent when compared to similar ligands without these groups.

Of interest was that the SAR on the E ring appeared not to be explained by the docking simulations. Most different ring E variants docked well into the binding site and showed comparable docking scores, supporting the notion that the site occupied by this ring is dominated by hydrophobic interactions and allows for promiscuous occupancy by various functional groups on the E ring. This supports the data in Table 2 which show very little fluctuation in the bioactivities of the compound sets 18–25 and 26–33, these compounds only differing in the substitution of the E ring.

Only the enantiomer matching the absolute configuration of podophyllotoxin shows potent anticancer activity and good docking properties. Importantly, the modeling study led to the observation that the stereochemical arrangement at carbon C-1 (podophyllotoxin numbering, Figure 1) was critical to the ability of the MCR products to overlap with the podophyllotoxin ligand. The docking results showed that compounds with the “wrong” configuration, relative to the *R* configuration of podophyllotoxin, did not dock well at all; in fact a “flip” of the BCD or ABCD core of the MCR product was often required to afford a satisfactory fit. For example, Figure 7 depicts the best docking fit of *R*-19 (Figure 7A) and *S*-19 (Figure 7D), respectively. *R*-19 nicely overlaps with podophyllotoxin (Figure 7A), while *S*-19 shows a very poor overlay with the natural product (Figure 7D); of significance is that the modeling

predicted the majority of the “best fits” for this molecule to require a “flip” of the compound in the binding site as shown in the Figure 7D.

Next, we investigated if this predicted difference in docking propensity would translate into an actual difference in the bioactivities of the different enantiomers. To this end, compound 19 was chosen for closer examination, as the naphthalene moiety and two bromine atoms were expected to assist in the subsequent single crystal X-ray diffraction studies. A sample of 19 was therefore separated into its enantiomers *R*-19 and *S*-19 by chiral HPLC (see Supporting Information). Subsequent biochemical evaluation of the two compounds confirmed that one optical antipode was indeed much more potent (see Figure 8). A larger scale HPLC separation then gave in hand sufficient amounts of *R*-19 and *S*-19 such that crystals could be obtained for the less potent enantiomer. These were then duly analyzed by X-ray crystallography to confirm that this antipode had the *S* stereochemistry (Figure 8). These results further support the favored binding of the *R*-MCR derivatives to the active site of tubulin, which is responsible for the higher potency observed for the *R*-enantiomer. Furthermore, this corroborated the hypothesis that our compounds, synthesized in a single step, were interacting with tubulin in a similar manner to podophyllotoxin.

CONCLUSIONS

In summary, notwithstanding their significantly simpler structures, several heterocyclic podophyllotoxin-mimetic libraries rival the parent natural product by exhibiting nanomolar antiproliferative activities against human cancer cells and manifesting potent apoptosis inducing properties. At present such libraries include compounds based on dihydropyridopyrazole, dihydropyridonaphthalene, dihydropyridoindole, and dihydropyridopyrimidine scaffolds. These promising discoveries and the computer modeling results together indicate that potent activities may be found in many related, but yet unexplored, podophyllotoxin-mimetic heterocycles that can be prepared using the MCR process described in this investigation. Importantly, using the dihydropyridopyrazole compounds, we demonstrated that, in a manner similar to podophyllotoxin, these heterocycles inhibit *in vitro* tubulin polymerization and disrupt the formation of mitotic spindle in dividing cells at low nanomolar concentrations, thus attesting to their bona fide mimicry of podophyllotoxin. This is further corroborated by separation of a potent racemic dihydropyridonaphthalene compound into individual enantiomers and demonstration of high potency associated only with the enantiomer matching the absolute configuration of podophyllotoxin, an outcome predicted by computer modeling. Altogether, the results of this study present a strong case for the utilization of a mimetic scaffold approach as a useful paradigm in drug discovery.

EXPERIMENTAL SECTION

General Synthetic Methods. All aldehydes, aminopyrazoles, ethanol, and tetric acid were purchased from commercial sources and used without purification. Triethylamine (Et_3N) was distilled from CaH_2 . All reactions were performed in a reaction vessel open to the atmosphere and monitored by thin layer chromatography (TLC) on pre-coated (250 μm) silica gel 60F₂₅₄ glass-backed plates. Visualization was accomplished with UV light and aqueous ceric ammonium molybdate solution or potassium permanganate stain followed by charring on a hot plate. Flash column chromatography was performed on silica gel (32–63 μm , 60 Å pore size). 1H and ^{13}C NMR spectra were recorded on

a Jeol Eclipse 300 or Bruker Avance III 400 spectrometer. Chemical shifts (δ) are reported in ppm relative to the TMS internal standard. Abbreviations are as follows: s (singlet), d (doublet), dd (doublet of doublets), t (triplet), q (quartet), m (multiplet). HRMS analyses were performed at the Mass Spectrometry Facility, University of New Mexico. Samples were run on LCT Premier TOF mass spectrometer. The synthesized compounds are at least 95% pure according to HPLC analysis.

General Procedure for Dihydropyridopyrazole Synthesis. A mixture of 5-aminopyrazole or 5-amino-3-methylpyrazole (1 mmol), tetrionic acid (1 mmol), triethylamine (0.05 mL), and a corresponding aldehyde (1 mmol) in EtOH (4 mL) was refluxed for 0.5–3 h. The reaction mixture was allowed to cool to room temperature, and the precipitated product was collected by vacuum filtration and washed with EtOH (3 mL) at room temperature. In most cases, the products were >98% pure as judged by NMR analysis. When an impurity was present, the product was recrystallized from DMF/H₂O.

4-(3,4,5-Trimethoxyphenyl)-1,4,7,8-tetrahydro-5H-furo[3,4-b]pyrazolo[4,3-e]pyridin-5-one (2). 75% yield as white solid, mp = 262–263 °C. ¹H NMR (DMSO-*d*₆) δ 3.79 (s, 9H), 4.85–5.00 (dd, *J* = 15 Hz, 2H), 4.92 (s, 1H), 6.48 (s, 2H), 7.40 (s, 1H), 10.21 (s, 1H), 12.18 (s, 1H); ¹³C NMR (DMSO-*d*₆) δ 172.6, 160.6, 153.1, 147.8, 141.5, 136.6, 136.4, 105.5, 102.8, 96.0, 60.5, 56.4, 56.3; HRMS *m/z* (ESI) calcd for C₁₇H₁₈N₃O₅ (M + H)⁺ 344.1246, found 344.1238.

4-(3-Bromo-4,5-dimethoxyphenyl)-1,4,7,8-tetrahydro-5H-furo[3,4-b]pyrazolo[4,3-e]pyridin-5-one (4). 72% yield as white solid, mp = 244–246 °C. ¹H NMR (DMSO-*d*₆) δ 3.67 (s, 3H, OCH₃), 3.79 (s, 3H, OCH₃), 4.80–5.11 (m, 3H, CH + CH₂), 6.82 (s, 1H, CH_{Ar}), 6.98 (s, 1H, CH_{Ar}), 7.40 (s, 1H, CH_{pyr}), 10.27 (s, 1H, NH), 12.24 (s, 1H, NH); ¹³C NMR (DMSO-*d*₆) δ 172.6 (C=O), 161.2 (C_{Ar}), 153.7 (C_{Ar}), 144.7 (C_{Ar}), 144.0 (C_{Ar}), 122.9 (C_{Ar}), 116.9 (C_{Ar}), 112.6 (C_{Ar}), 112.5 (C_{Ar}), 105.5 (C_{pyr}), 95.2 (C=C–NH), 65.6 (OCH₂), 60.5 (OCH₃), 56.6 (OCH₃), 34.5 (CH); HRMS *m/z* (ESI) calcd for C₁₆H₁₄BrN₃O₄Na (M + Na)⁺ 414.0065, found 414.0058.

4-(3-Bromophenyl)-1,4,7,8-tetrahydro-5H-furo[3,4-b]pyrazolo[4,3-e]pyridin-5-one (6). 71% yield as white solid, mp = 294–296 °C. ¹H NMR (DMSO-*d*₆) δ 4.81–5.01 (m, 3H), 7.23 (s, 1H), 7.35 (s, 4H), 10.29 (s, 1H), 12.25 (s, 1H); ¹³C NMR (DMSO-*d*₆) δ 172.4, 161.1, 149.2, 130.9, 130.5, 130.4, 129.6, 121.4, 105.5, 95.3, 65.6, 35.6; HRMS *m/z* (ESI) calcd for C₁₄H₁₀BrN₃O₂Na (M + Na)⁺, 353.9854, found 353.9859.

4-(5-Bromo-3-pyridinyl)-3-methyl-1,4,7,8-tetrahydro-5H-furo[3,4-b]pyrazolo[4,3-e]pyridin-5-one (7). 88% yield as white solid, mp \geq 300 °C. ¹H NMR (DMSO-*d*₆) δ 1.78 (s, 3H), 4.84–4.93 (dd, *J* = 15 Hz, 2H), 4.98 (s, 1H), 7.77 (d, *J* = 1.9 Hz, 1H), 8.46 (d, *J* = 1.9 Hz, 1H), 8.52 (d, 1H, *J* = 1.9 Hz), 10.28 (s, 1H), 12.04 (s, 1H); ¹³C NMR (DMSO-*d*₆) δ 172.9, 161.4, 149.4, 147.7, 143.2, 137.9, 121.5, 101.1, 94.9, 65.6, 32.3, 10.2; HRMS *m/z* (ESI) calcd for C₁₄H₁₁BrN₄O₂Na (M + Na)⁺ 368.9963, found 368.9963.

4-(5-Bromo-3-pyridinyl)-1,4,7,8-tetrahydro-5H-furo[3,4-b]pyrazolo[4,3-e]pyridin-5-one (8). 76% yield as white solid, mp = 283–284 °C. ¹H NMR (DMSO-*d*₆) δ 4.80–5.02 (m, 3H), 5.02 (s, 1H), 7.37 (s, 1H), 7.73 (s, 1H), 8.43 (s, 1H), 8.47 (s, 1H), 10.33 (s, 1H), 12.28 (s, 1H); ¹³C NMR (DMSO-*d*₆) δ 172.9, 161.6, 149.4, 147.6, 143.6, 138.3, 129.4, 120.9, 104.1, 93.9, 65.5, 32.2; HRMS *m/z* (ESI) calcd for C₁₂H₉BrN₄O₂Na (M + Na)⁺ 354.9807, found 354.9807.

4-(3,5-Dibromophenyl)-3-methyl-1,4,7,8-tetrahydro-5H-furo[3,4-b]pyrazolo[4,3-e]pyridin-5-one (9). 85% yield as white solid, mp = 290–292 °C. ¹H NMR (DMSO-*d*₆) δ 1.89 (s, 3H), 4.80–5.02 (m, 3H), 7.39 (s, 2H), 7.64 (s, 1H), 10.28 (s, 1H), 12.04 (s, 1H); ¹³C NMR (DMSO-*d*₆) δ 172.5, 161.1, 150.3, 147.4, 137.0, 130.2, 122.8, 101.9, 95.1, 65.4, 34.5, 10.2; HRMS *m/z* (ESI) calcd for C₁₅H₁₁Br₂N₃O₂Na (M + Na)⁺ 445.9116, found 445.9109.

4-(3,5-Dibromophenyl)-1,4,7,8-tetrahydro-5H-furo[3,4-b]pyrazolo[4,3-e]pyridin-5-one (10). 83% yield as white solid,

mp = 268–270 °C. ¹H NMR (DMSO-*d*₆) δ 4.82–5.06 (m, 3H), 7.38 (s, 3H), 7.62 (s, 1H), 10.36 (s, 1H), 12.29 (s, 1H); ¹³C NMR (DMSO-*d*₆) δ 172.7, 161.7, 151.5, 147.2, 130.4, 122.9, 104.4, 95.2, 65.5, 34.6; HRMS *m/z* (ESI) calcd for C₁₄H₉Br₂N₃O₂Na (M + Na)⁺ 431.8959, found 431.8952.

4-(5-Bromo-2-hydroxy-3-methoxyphenyl)-3-methyl-1,4,7,8-tetrahydro-5H-furo[3,4-b]pyrazolo[4,3-e]pyridin-5-one (11). 85% yield as yellow solid, mp = 255–256 °C. ¹H NMR (DMSO-*d*₆) δ 1.85 (s, 3H), 3.80 (s, 3H), 4.77–4.95 (dd, *J* = 15 Hz, 2H), 5.20 (s, 1H), 6.57 (s, 1H), 6.89 (s, 1H), 8.96 (s, 1H), 10.09 (s, 1H), 11.85 (s, 1H); ¹³C NMR (DMSO-*d*₆) δ 172.3, 161.7, 148.9, 143.1, 136.9, 124.1, 113.0, 110.4, 103.3, 95.7, 56.8, 31.1, 10.3; HRMS *m/z* (ESI) calcd for C₁₆H₁₄BrN₃O₄Na (M + Na)⁺ 414.0065, found 414.0051.

4-(5-Bromo-2-hydroxy-3-methoxyphenyl)-1,4,7,8-tetrahydro-5H-furo[3,4-b]pyrazolo[4,3-e]pyridin-5-one (12). 81% yield as pink solid, mp = 248–250 °C. ¹H NMR (DMSO-*d*₆) δ 3.79 (s, 3H), 4.82–5.04 (dd, *J* = 15 Hz, 2H), 5.22 (s, 1H), 6.53 (s, 1H), 6.92 (s, 1H), 7.28 (s, 1H), 8.99 (s, 1H), 10.17 (s, 1H), 12.06 (s, 1H); ¹³C NMR (DMSO-*d*₆) δ 173.8, 162.3, 149.9, 142.9, 135.4, 122.6, 113.3, 110.7, 105.8, 93.9, 65.2, 56.8, 28.6; HRMS *m/z* (ESI) calcd for C₁₅H₁₂BrN₃O₄Na (M + Na)⁺ 399.9909, found 399.9905.

4-(5-Bromo-2-hydroxyphenyl)-3-methyl-1,4,7,8-tetrahydro-5H-furo[3,4-b]pyrazolo[4,3-e]pyridin-5-one (13). 83% yield as white solid, mp = 260–262 °C. ¹H NMR (DMSO-*d*₆) δ 1.82 (s, 3H), 4.78–4.98 (dd, *J* = 15 Hz, 2H), 5.15 (s, 1H), 6.73 (d, *J* = 6.3 Hz, 1H), 6.94 (s, 1H), 9.77 (s, 1H), 7.11 (d, *J* = 6.3 Hz, 1H), 9.77 (s, 1H), 10.07 (s, 1H), 11.84 (s, 1H); ¹³C NMR (DMSO-*d*₆) δ 172.5, 161.1, 153.8, 147.6, 135.2, 132.2, 130.0, 118.2, 111.0, 103.4, 96.0, 65.6, 27.7, 10.5; HRMS *m/z* (ESI) calcd for C₁₅H₁₂BrN₃O₃Na (M + Na)⁺ 383.9960, found 383.9962.

4-(5-Bromo-2-hydroxyphenyl)-1,4,7,8-tetrahydro-5H-furo[3,4-b]pyrazolo[4,3-e]pyridin-5-one (14). 74% yield as white solid, mp = 243–244 °C. ¹H NMR (DMSO-*d*₆) δ 4.84–5.08 (dd, *J* = 15 Hz, 2H), 5.18 (s, 1H), 6.78 (d, *J* = 8.4 Hz, 1H), 6.91 (d, *J* = 2.3 Hz, 1H), 7.13 (dd, *J* = 2.3, 8.4 Hz, 1H), 7.33 (s, 1H), 9.92 (s, 1H), 10.20 (s, 1H), 12.12 (s, 1H); ¹³C NMR (DMSO-*d*₆) δ 172.6, 162.2, 153.9, 135.4, 130.7, 130.1, 118.2, 110.9, 105.9, 94.2, 65.8, 28.8; HRMS *m/z* (ESI) calcd for C₁₄H₁₀BrN₃O₃Na (M + Na)⁺ 369.9803, found 369.9815.

4-(2-Hydroxy-3-methoxyphenyl)-1,4,7,8-tetrahydro-5H-furo[3,4-b]pyrazolo[4,3-e]pyridin-5-one (15). 70% yield as white solid, mp = 276–278 °C. ¹H NMR (DMSO-*d*₆) δ 3.78 (s, 3H), 4.89 (m, 2H), 4.89 (s, 1H), 5.23 (s, 1H), 6.47 (m, 1H), 6.64 (m, 1H), 6.75 (m, 1H), 7.31 (s, 1H), 8.65 (s, 1H), 10.13 (s, 1H), 12.05 (s, 1H); ¹³C NMR (DMSO-*d*₆) δ 172.7, 161.8, 148.3, 143.4, 133.4, 120.2, 119.3, 110.3, 106.6, 95.0, 65.7, 56.5, 28.6; HRMS *m/z* (ESI) calcd for C₁₅H₁₃N₃O₄Na (M + Na)⁺ 322.0804, found 322.0803.

4-(3,5-Dibromo-2-hydroxyphenyl)-1,4,7,8-tetrahydro-5H-furo[3,4-b]pyrazolo[4,3-e]pyridin-5-one (16). 76% yield as white solid, mp = 252–254 °C. ¹H NMR (DMSO-*d*₆) δ 4.82–5.03 (dd, *J* = 15 Hz, 2H), 5.34 (s, 1H), 6.96 (d, *J* = 1.2 Hz, 1H), 7.34 (s, 1H), 7.50 (d, *J* = 1.2 Hz, 1H), 9.43 (s, 1H), 10.19 (s, 1H), 12.10 (s, 1H); ¹³C NMR (DMSO-*d*₆) δ 172.8, 162.1, 150.8, 138.4, 132.6, 130.7, 113.7, 112.3, 105.1, 95.2, 66.0, 29.7; HRMS *m/z* (ESI) calcd for C₁₄H₉Br₂N₃O₃Na (M + Na)⁺ 447.8908, found 447.8901.

4-(4-Bromo-2-thienyl)-1,4,7,8-tetrahydro-5H-furo[3,4-b]pyrazolo[4,3-e]pyridin-5-one (17). 10% yield as pink solid, mp = 264–266 °C. ¹H NMR (DMSO-*d*₆) δ 4.81–4.93 (dd, *J* = 15 Hz, 2H), 5.30 (s, 1H), 6.98 (s, 1H), 7.43 (s, 1H), 7.55 (s, 1H), 10.4 (s, 1H), 12.37 (s, 1H). ¹³C NMR (DMSO-*d*₆) δ 30.2, 65.4, 94.7, 104.7, 108.4, 122.2, 126.2, 128.2, 146.8, 153.0, 160.8, 172.3; HRMS *m/z* (ESI) calcd for C₁₂H₈BrN₃O₂Na (M + Na)⁺ 361.9575, found 361.9566.

General Procedure for the Other Heterocyclic Scaffold Synthesis. A mixture of a selected amino derivative (1 mmol), tetrionic acid (1.1 mmol), and a corresponding aldehyde (1.1 mmol) in EtOH

(4 mL) was refluxed for 12–36 h. The reaction mixture was allowed to cool to room temperature, and the precipitated product was collected by vacuum filtration and washed with EtOH (3 mL) and Et₂O at room temperature. In several cases (34, 35, 37, 38, 39), the products were >98% pure as judged by NMR analysis. In the other cases, they were purified by flash chromatography on silica gel with the indicated solvent system.

7-(3,4,5-Trimethoxyphenyl)-7,11-dihydrobenzo[h]furo[3,4-b]quinolin-8(10H)-one (18). 14% yield as white solid, mp = 256–258 °C (CHCl₃/MeOH = 20/1). ¹H NMR (DMSO-*d*₆) δ 3.51 (s, 3H, OCH₃), 3.59 (s, 6H, OCH₃), 4.88–5.06 (m, 3H, CH + CH₂), 6.47 (s, 2H, CH_{Ar}), 7.13–7.52 (m, 4H, CH_{Naph}), 7.77 (d, *J* = 7.4 Hz, 1H, CH_{Naph}), 8.19 (d, 1H, *J* = 8.2 Hz, CH_{Naph}), 10.24 (s, 1H, NH); ¹³C NMR (DMSO-*d*₆) δ 56.3 (OCH₃), 60.4 (OCH₃), 66.2 (OCH₂), 96.7 (C=C–NH), 105.8 (C_{Ar}), 119.7 (C_{Ar}), 121.6 (C_{Ar}), 123.3 (C_{Ar}), 126.6 (C_{Ar}), 128.8 (C_{Ar}), 131.4 (C_{Ar}), 133.1 (C_{Ar}), 136.7 (C_{Ar}), 143.1 (C_{Ar}), 153.3 (C_{Ar}), 159.1 (C_{Ar}), 172.6 (C=O); HRMS *m/z* (ESI) calcd for C₂₄H₂₁NO₅Na (M + Na)⁺ 426.1317, found 426.1321.

7-(3,5-Dibromophenyl)-7,11-dihydrobenzo[h]furo[3,4-b]quinolin-8(10H)-one (19). 39% yield as pink solid, mp = more 300 °C (CHCl₃/MeOH = 20/1). ¹H NMR (DMSO-*d*₆) δ 4.88–5.09 (dd, *J* = 15 Hz, 2H), 5.31 (s, 1H), 7.17 (d, *J* = 9.0 Hz, 1H), 7.48–7.61 (m, 6H), 7.86 (d, *J* = 6 Hz, 1H), 8.24 (d, *J* = 9 Hz, 1H), 10.33 (s, 1H); ¹³C NMR (DMSO-*d*₆) δ 69.9, 114.8, 122.3, 122.6, 123.8, 125.1, 128.0, 128.9, 130.0, 130.3, 131.5, 134.0, 134.1, 136.2, 145.2, 149.6, 163.9, 167.9; HRMS *m/z* (ESI) calcd for C₂₁H₁₃Br₂NO₂Na (M + Na)⁺ 491.9211, found 491.9216.

7-(3-Bromo-4,5-dimethoxyphenyl)-7,11-dihydrobenzo[h]furo[3,4-b]quinolin-8(10H)-one (20). 22% yield as yellow solid, mp = 276–278 °C (CHCl₃/MeOH = 20/1). ¹H NMR (DMSO-*d*₆) δ 3.69 (s, 3H), 3.76 (s, 3H), 4.91–5.17 (m, 3H), 6.84 (s, 1H), 7.06 (s, 1H), 7.20 (d, *J* = 6 Hz, 1H), 7.45–7.83 (m, 3H), 7.83 (d, *J* = 9 Hz, 1H), 8.19 (d, *J* = 9.0 Hz), 10.23 (s, 1H); ¹³C NMR (DMSO-*d*₆) δ 56.6, 60.5, 66.3, 96.4, 112.8, 117.3, 119.2, 121.5, 123.1, 123.5, 123.8, 126.8, 128.8, 131.5, 133.2, 144.7, 144.9, 153.7, 159.3, 172.6; HRMS *m/z* (ESI) calcd for C₂₃H₁₈BrNO₄Na (M + Na)⁺ 474.0317, found 474.0311.

7-(3,5-Dibromo-2-hydroxyphenyl)-7,11-dihydrobenzo[h]furo[3,4-b]quinolin-8(10H)-one (21). 41% yield as white solid, mp = 160–162 °C (CHCl₃/MeOH = 20/1). ¹H NMR (DMSO-*d*₆) δ 4.97–5.16 (dd, *J* = 15 Hz, 2H), 5.69 (s, 1H), 7.46–7.17 (m, 2H), 7.46–7.64 (m, 4H), 7.85 (d, *J* = 9 Hz, 1H), 7.95 (s, 1H), 8.21 (d, *J* = 9 Hz, 1H), 9.73 (s, 1H), 10.34 (s, 1H); ¹³C NMR (DMSO-*d*₆) δ 34.5, 66.5, 70.4, 95.7, 112.3, 113.8, 116.2, 119.5, 121.4, 123.6, 126.7, 128.0, 128.7, 130.6, 131.4, 132.3, 133.1, 139.1, 150.6, 160.0, 164.4, 172.6; HRMS *m/z* (ESI) calcd for C₂₁H₁₃Br₂NO₃Na (M + Na)⁺ 507.9160, found 507.9160.

7-(5-Bromo-2-hydroxy-3-methoxyphenyl)-7,11-dihydrobenzo[h]furo[3,4-b]quinolin-8(10H)-one (22). 74% yield as white solid, mp = 276–278 °C (CHCl₃/MeOH = 20/1). ¹H NMR (DMSO-*d*₆) δ 3.73 (s, 3H), 4.87–5.08 (dd, *J* = 15 Hz, 2H), 5.54 (s, 1H), 6.64 (s, 1H), 6.84 (s, 1H), 7.15–7.52 (m, 4H), 7.72–7.78 (m, 1H), 8.12 (d, *J* = 9 Hz, 1H), 9.08 (s, 1H), 10.12 (s, 1H); ¹³C NMR (DMSO-*d*₆) δ 33.2, 56.7, 66.3, 95.9, 110.7, 113.2, 120.4, 121.4, 123.0, 123.5, 124.1, 126.7, 128.2, 128.7, 131.1, 133.1, 136.1, 142.7, 149.2, 159.9, 172.5; HRMS *m/z* (ESI) calcd for C₂₂H₁₇BrNO₄ (M + H)⁺ 438.0341, found 438.0346.

7-(5-Bromo-2-hydroxyphenyl)-7,11-dihydrobenzo[h]furo[3,4-b]quinolin-8(10H)-one (23). 68% yield as pink solid, mp = 95–97 °C (CHCl₃/MeOH = 20/1). ¹H NMR (DMSO-*d*₆) δ 4.86–5.07 (dd, *J* = 15 Hz, 2H), 5.46 (s, 1H), 6.71 (d, 9.0 Hz, 1H), 7.00–7.19 (m, 3H), 7.35–7.51 (m, 3H), 7.74 (d, *J* = 8.0 Hz, 1H), 8.20 (d, *J* = 9.0 Hz, 1H), 9.89 (s, 1H), 10.01 (s, 1H); ¹³C NMR (DMSO-*d*₆) δ 33.4, 66.27, 95.91, 111.0, 118.2, 120.4, 121.4, 123.0, 123.5, 126.7, 128.2, 128.7, 130.6, 131.2, 132.5, 133.1, 136.6, 153.6, 160.4, 172.5; HRMS *m/z* (ESI) calcd for C₂₁H₁₄BrNO₃Na (M + Na)⁺ 430.0055, found 430.0050.

7-(5-Bromo-3-pyridinyl)-7,11-dihydrobenzo[h]furo[3,4-b]quinolin-8(10H)-one (24). 35% yield as white solid, mp = 262–264 °C, dec (CHCl₃/MeOH = 20/1). ¹H NMR (DMSO-*d*₆) δ 4.97–5.15 (dd, *J* = 15 Hz, 2H), 5.35 (s, 1H), 7.16 (d, *J* = 9 Hz, 1H), 7.49–7.65 (m, 3H), 7.84–7.87 (m, 2H), 8.28 (d, *J* = 9.0 Hz, 1H), 8.52–8.55 (m, 2H); ¹³C NMR (DMSO-*d*₆) δ 37.9, 66.6, 95.5, 118.2, 121.1, 121.8, 123.2, 123.8, 127.0, 127.1, 128.6, 128.9, 131.9, 133.3, 138.4, 144.4, 148.3, 149.1, 159.8, 172.5; HRMS *m/z* (ESI) calcd for C₂₀H₁₃BrN₂O₂Na (M + Na)⁺ 415.0058, found 415.0054.

7-(4-Bromo-2-thienyl)-7,11-dihydrobenzo[h]furo[3,4-b]quinolin-8(10H)-one (25). 56% yield as yellow solid, mp = 268–269 °C (CHCl₃/MeOH = 20/1). ¹H NMR (DMSO-*d*₆) δ 4.96–5.12 (dd, *J* = 15 Hz, 2H), 5.54 (s, 1H), 7.04 (s, 1H), 7.33–7.64 (m, 5H), 7.89 (d, *J* = 9 Hz, 1H), 8.21 (d, *J* = 9 Hz, 1H), 10.38 (s, 1H); ¹³C NMR (DMSO-*d*₆) δ 35.6, 66.2, 95.9, 108.7, 118.5, 121.4, 123.0, 123.2, 123.7, 126.6, 127.0, 128.6, 128.8, 131.2, 133.3, 153.4, 159.2, 172.3; HRMS *m/z* (ESI) calcd for C₁₉H₁₂BrNO₂SK (M + K)⁺ 435.9409, found 435.9414.

2-Hydroxy-7-(3,4,5-trimethoxyphenyl)-7,11-dihydrobenzo[h]furo[3,4-b]quinolin-8(10H)-one (26). 63% yield as white solid, mp ≥ 300 °C (CHCl₃/MeOH = 20/1). ¹H NMR (DMSO-*d*₆) δ 3.77 (s, 6H, OCH₃), 3.67 (s, 3H, OCH₃), 4.97–5.10 (m, 3H, CH + CH₂), 6.53 (s, 2H, CH_{Ar}), 7.02 (d, *J* = 9.0 Hz, 1H, CH_{Naph}), 7.13 (d, *J* = 9.0 Hz, 1H, CH_{Naph}), 7.37 (d, *J* = 9.0 Hz, 1H, CH_{Naph}), 7.42 (s, 1H, CH_{Naph}), 7.70 (d, *J* = 9 Hz, 1H, CH_{Naph}), 9.84 (s, 1H, OH), 9.98 (s, 1H, NH); ¹³C NMR (DMSO-*d*₆) δ 56.3 (OCH₃), 60.4 (OCH₃), 66.2 (OCH₂), 96.4 (C=C–NH), 103.9 (C_{Ar}), 105.7 (C_{Ar}), 118.8 (C_{Ar}), 119.8 (C_{Ar}), 123.2 (C_{Ar}), 124.8 (C_{Ar}), 125.4 (C_{Ar}), 127.6 (C_{Ar}), 129.9 (C_{Ar}), 130.3 (C_{Ar}), 136.6 (C_{Ar}), 143.2 (C_{Ar}), 153.3 (C_{Ar}), 156.3 (C_{Ar}), 159.2 (C_{Ar}), 172.7 (C=O); HRMS *m/z* (ESI) calcd for C₂₄H₂₁NO₆Na (M + Na)⁺ 442.1267, found 442.1267.

7-(3,5-Dibromophenyl)-2-hydroxy-7,11-dihydrobenzo[h]furo[3,4-b]quinolin-8(10H)-one (27). 50% yield as yellow solid, mp ≥ 300 °C (CHCl₃/MeOH = 20/1). ¹H NMR (DMSO-*d*₆) δ 4.92–5.12 (dd, *J* = 15 Hz, 2H), 5.24 (s, 1H), 6.88 (d, *J* = 9.0 Hz, 1H), 7.16 (d, *J* = 9.0 Hz, 1H), 7.37–7.71 (m, 6H), 9.90 (s, 1H), 10.09 (s, 1H); ¹³C NMR (DMSO-*d*₆) δ 66.5, 95.5, 103.9, 118.6, 119.2, 123.2, 123.8, 125.2, 130.3, 130.5, 132.1, 151.6, 159.7, 172.6; HRMS *m/z* (ESI) calcd for C₂₁H₁₃Br₂NO₃Na (M + Na)⁺ 507.9160, found 507.9160.

7-(3-Bromo-4,5-dimethoxyphenyl)-2-hydroxy-7,11-dihydrobenzo[h]furo[3,4-b]quinolin-8(10H)-one (28). 34% yield as yellow solid, mp ≥ 300 °C (CHCl₃/MeOH = 20/1). ¹H NMR (DMSO-*d*₆) δ 3.67 (s, 3H), 3.80 (s, 3H), 4.94–5.12 (dd, *J* = 15 Hz, 2H), 5.16 (s, 1H), 6.85 (s, 1H), 6.99 (d, *J* = 9.0 Hz, 1H), 7.08 (s, 1H), 7.16 (d, *J* = 9.0 Hz, 1H), 7.40 (d, *J* = 9.0 Hz, 1H), 7.44 (s, 1H), 7.72 (d, *J* = 9.0 Hz, 1H), 9.88 (s, 1H), 10.05 (s, 1H); ¹³C NMR (DMSO-*d*₆) δ 40.9, 56.5, 60.4, 66.2, 96.0, 103.8, 112.7, 117.2, 118.9, 119.2, 123.4, 124.8, 125.3, 130.0, 130.3, 144.5, 144.9, 153.6, 156.4, 159.3, 172.6; HRMS *m/z* (ESI) calcd for C₂₁H₁₃Br₂NO₄Na (M + Na)⁺ 490.0266, found 490.0268.

7-(3,5-Dibromo-2-hydroxyphenyl)-2-hydroxy-7,11-dihydrobenzo[h]furo[3,4-b]quinolin-8(10H)-one (29). 42% yield as yellow solid, mp = 278–279 °C (CHCl₃/MeOH = 20/1). ¹H NMR (DMSO-*d*₆) δ 4.82–5.01 (dd, *J* = 15 Hz, 2H), 5.56 (s, 1H), 6.78–7.57 (m, 7H), 9.61 (s, 1H), 9.74 (s, 1H), 9.91 (s, 1H); ¹³C NMR (DMSO-*d*₆) δ 34.6, 66.5, 95.4, 103.7, 112.2, 118.9, 119.7, 123.6, 124.6, 124.7, 127.7, 129.9, 130.3, 132.3, 132.9, 139.2, 150.5, 156.5, 160.0, 172.8; HRMS *m/z* (ESI) calcd for C₂₁H₁₃Br₂NO₄Na (M + Na)⁺ 523.9109, found 523.9100.

7-(5-Bromo-2-hydroxy-3-methoxyphenyl)-2-hydroxy-7,11-dihydrobenzo[h]furo[3,4-b]quinolin-8(10H)-one (30). 58% yield as yellow solid, mp = 215–217 °C (CHCl₃/MeOH = 20/1). ¹H NMR (DMSO-*d*₆) δ 3.84 (s, 3H), 4.95–5.15 (dd, *J* = 15 Hz, 2H), 5.59 (s, 1H), 6.71 (d, *J* = 3.0 Hz, 1H), 6.94 (d, *J* = 3.0 Hz, 1H), 7.04 (d, *J* = 9.0 Hz, 1H), 7.15 (d, *J* = 9.0 Hz, 1H), 7.36 (d, *J* = 9.0 Hz, 1H), 7.43 (s, 1H), 7.70 (d, *J* = 9.0 Hz, 1H), 9.14 (s, 1H), 9.85 (s, 1H), 9.96 (s, 1H); ¹³C NMR (DMSO-*d*₆) δ 56.1, 65.7, 95.0, 103.2, 110.1, 112.5, 118.2, 120.0,

122.9, 123.5, 124.2, 127.1, 129.2, 129.7, 132.0, 135.7, 142.1, 148.6, 155.8, 159.5, 172.0; HRMS m/z (ESI) calcd for $C_{22}H_{16}BrNO_3Na$ ($M + Na$)⁺ 476.0110, found 476.0106.

7-(5-Bromo-2-hydroxyphenyl)-2-hydroxy-7,11-dihydrobenzo[h]furo[3,4-b]quinolin-8(10H)-one (31). 42% yield as orange solid, mp = 288–289 °C, dec (CHCl₃/MeOH = 20/1). ¹H NMR (DMSO-*d*₆) δ 4.92–5.13 (dd, *J* = 15 Hz, 2H), 5.51 (s, 1H), 6.79 (d, *J* = 6.0 Hz, 1H), 7.02–7.41 (m, 6H), 7.67 (d, *J* = 6.0 Hz, 1H), 9.80 (s, 1H), 9.93 (s, 1H); ¹³C NMR (DMSO-*d*₆) δ 33.4, 66.4, 95.7, 103.8, 110.0, 118.2, 118.9, 120.6, 123.5, 124.8, 127.7, 129.8, 130.3, 130.5, 132.5, 136.8, 153.6, 156.4, 160.1, 172.6; HRMS m/z (ESI) calcd for $C_{21}H_{14}BrNO_4Na$ ($M + Na$)⁺ 446.0004, found 446.0013.

7-(5-Bromo-3-pyridinyl)-2-hydroxy-7,11-dihydrobenzo[h]furo[3,4-b]quinolin-8(10H)-one (32). 28% yield as white solid, mp ≥ 300 °C, dec (CHCl₃/MeOH = 20/1); ¹H NMR (DMSO-*d*₆) δ 4.92–5.12 (dd, *J* = 15 Hz, 2H), 5.248 (s, 1H), 6.88 (d, *J* = 9.0 Hz, 1H), 7.16 (d, *J* = 9.0 Hz, 1H), 7.37–7.71 (m, 6H), 9.90 (s, 1H), 10.09 (s, 1H); ¹³C NMR (DMSO-*d*₆) δ 66.5, 95.5, 103.9, 118.6, 119.2, 123.2, 123.8, 125.2, 130.3, 130.5, 132.1, 151.6, 159.7, 172.6; HRMS m/z (ESI) calcd for $C_{23}H_{19}BrNO_5Na$ ($M + Na$)⁺ 490.0266, found 490.0268.

7-(4-Bromo-2-thienyl)-2-hydroxy-7,11-dihydrobenzo[h]furo[3,4-b]quinolin-8(10H)-one (33). 33% yield as yellow solid, mp = 273–274 °C (CHCl₃/MeOH = 20/1). ¹H NMR (DMSO-*d*₆) δ 4.92–5.09 (dd, *J* = 15 Hz, 2H), 5.48 (s, 1H), 7.01 (s, 1H), 7.08–7.16 (m, 2H), 7.41–7.44 (d, *J* = 7.0 Hz, 3H), 7.70 (d, *J* = 9.0 Hz, 1H), 9.88 (s, 1H), 10.15 (s, 1H); ¹³C NMR (DMSO-*d*₆) δ 35.8, 66.3, 95.6, 103.9, 108.7, 118.7, 119.2, 123.2, 123.7, 124.8, 125.2, 126.6, 129.9, 130.5, 153.6, 156.6, 159.3, 172.4; HRMS m/z (ESI) calcd for $C_{19}H_{12}BrNO_3SNa$ ($M + Na$)⁺ 435.9619, found 435.9623.

4-Hydroxy-7-(3,4,5-trimethoxyphenyl)-7,11-dihydrobenzo[h]furo[3,4-b]quinolin-8(10H)-one (34). 59% yield as brown solid, mp = 300 °C. ¹H NMR (DMSO-*d*₆) δ 3.59 (s, 3H, OCH₃), 3.69 (s, 6H, OCH₃), 4.93–5.09 (dd, *J* = 15 Hz, 2H, CH₂), 5.48 (s, 1H, CH), 6.53 (s, 2H, CH_{Ar}), 6.88 (d, *J* = 7.1, CH_{Ar}), 7.37 (d, *J* = 8.8 Hz, 1H, CH_{Ar}), 7.38 (t, *J* = 8.3 Hz, 1H, CH_{Ar}), 7.61 (d, *J* = 8.5 Hz, 1H, CH_{Ar}), 7.71 (d, *J* = 8.5 Hz, 1H, CH_{Ar}), 10.05 (s, 1H, OH), 10.15 (s, 1H, NH); ¹³C NMR (DMSO-*d*₆) δ 56.3 (OCH₃), 60.4 (OCH₃), 66.2 (OCH₂), 96.6 (C=C–NH), 105.8 (C_{Ar}), 109.1 (C_{Ar}), 112.0 (C_{Ar}), 117.5 (C_{Ar}), 119.9 (C_{Ar}), 124.6 (C_{Ar}), 127.2 (C_{Ar}), 127.3 (C_{Ar}), 131.1 (C_{Ar}), 136.7 (C_{Ar}), 143.1 (C_{Ar}), 153.3 (C_{Ar}), 154.1 (C_{Ar}), 159.1 (C_{Ar}), 172.7 (C=O); HRMS m/z (ESI) calcd for $C_{24}H_{21}NO_6Na$ ($M + Na$)⁺ 442.1267, found 442.1273.

7-(3,5-Dibromophenyl)-4-hydroxy-7,11-dihydrobenzo[h]furo[3,4-b]quinolin-8(10H)-one (35). 77% yield as brown solid, mp ≥ 300 °C. ¹H NMR (DMSO-*d*₆) δ 4.91–5.11 (dd, *J* = 15 Hz, 2H), 5.25 (s, 1H), 6.90 (d, *J* = 9.0 Hz, 1H), 7.04 (d, *J* = 9.0 Hz, 1H), 7.36–7.72 (m, 6H), 10.15 (s, 1H), 10.21 (s, 1H); ¹³C NMR (DMSO-*d*₆) δ 66.5, 95.7, 109.4, 112.0, 118.0, 118.6, 123.2, 124.7, 127.1, 127.6, 130.5, 131.5, 132.1, 151.8, 154.2, 160.0, 172.6; HRMS m/z (ESI) calcd for $C_{21}H_{13}Br_2NO_3Na$ ($M + Na$)⁺ 507.9160, found 507.9152.

5-Amino-7-(3,5-dibromophenyl)-7,11-dihydrobenzo[h]furo[3,4-b]quinolin-8(10H)-one (37). 66% yield as brown solid, mp = 242–244 °C, dec. ¹H NMR (DMSO-*d*₆) δ 4.76–5.02 (dd, *J* = 15 Hz, 2H, CH₂), 5.34 (s, 1H, CH), 6.14 (s, 1H, CH_{Naph}), 7.27–7.30 (m, 5H, CH_{Ar}), 7.91–7.70 (m, 3H, CH_{Ar}), 9.88 (s, 1H, NH); ¹³C NMR (DMSO-*d*₆) δ 66.1 (OCH₂), 93.6 (C=C–NH), 109.3 (C_{Ar}), 119.8 (C_{Ar}), 121.4 (C_{Ar}), 121.6 (C_{Ar}), 123.0 (C_{Ar}), 123.1 (C_{Ar}), 123.5 (C_{Ar}), 124.0 (C_{Ar}), 124.9 (C_{Ar}), 126.7 (C_{Ar}), 130.5 (C_{Ar}), 131.8 (C_{Ar}), 141.4 (C_{Ar}), 151.8 (C_{Ar}), 158.7 (C_{Ar}), 172.7 (C=O); HRMS m/z (ESI) calcd for $C_{21}H_{15}Br_2N_2O_2$ ($M + H$)⁺ 484.9500, found 484.9492.

11-(3,4,5-Trimethoxyphenyl)-8,11-dihydrobenzo[f]furo[3,4-b]quinolin-10(7H)-one (38). 62% yield as white solid, mp = 263–264 °C; ¹H NMR (DMSO-*d*₆) δ 3.55 (s, 3H), 3.58 (s, 6H), 4.92–5.02 (dd, *J* = 15 Hz, 2H, CH₂), 5.64 (s, 1H, CH), 6.47 (s, 2H,

CH_{Ar}), 7.28–7.42 (m, 3H, CH_{Naph}), 7.85–7.88 (m, 3H, CH_{Naph}), 10.28 (s, 1H, NH); ¹³C NMR (DMSO-*d*₆) δ 36.8 (CH), 56.2 (OCH₃), 60.1 (OCH₃), 65.4 (OCH₂), 97.6 (C=C–NH), 105.7 (C_{Ar}), 115.0 (C_{Ar}), 118.1 (C_{Ar}), 123.7 (C_{Ar}), 124.3 (C_{Ar}), 127.3 (C_{Ar}), 128.6 (C_{Ar}), 129.4 (C_{Ar}), 131.1 (C_{Ar}), 132.5 (C_{Ar}), 135.2 (C_{Ar}), 136.1 (C_{Ar}), 142.0 (C_{Ar}), 153.3 (C_{Ar}), 157.6 (C_{Ar}), 172.6 (C=O); HRMS m/z (ESI) calcd for $C_{24}H_{21}NO_5Na$ ($M + Na$)⁺ 426.1317, found 426.1309.

11-(3,5-Dibromophenyl)-8,11-dihydrobenzo[f]furo[3,4-b]quinolin-10(7H)-one (39). 78% yield as pink solid, mp = 294–296 °C; ¹H NMR (DMSO-*d*₆) δ 4.77–4.94 (dd, *J* = 15 Hz, 2H), 5.68 (s, 1H), 7.18–7.79 (m, 9H), 10.30 (s, 1H); ¹³C NMR (DMSO-*d*₆) δ 36.9, 65.7, 96.5, 113.6, 118.1, 122.9, 123.5, 124.6, 127.6, 129.0, 130.1, 131.2, 131.8, 131.9, 135.6, 150.4, 158.1, 172.3; HRMS m/z (ESI) calcd for $C_{21}H_{14}Br_2NO_2$ ($M + H$)⁺ 469.9391, found 469.9386.

11-(3,4,5-Trimethoxyphenyl)-4,6,7,8,9,11-hexahydrobenzo[g]furo[3,4-b]quinolin-1(3H)-one (40). 13% yield as yellow solid, mp = 248–249 °C, dec (CHCl₃/MeOH = 20/1). ¹H NMR (DMSO-*d*₆) δ 1.55 (m, 4H, CH₂), 2.40–2.43 (m, 4H, CH₂), 3.48 (s, 3H, OCH₃), 3.59 (s, 6H, OCH₃), 4.71–4.91 (m, 3H, CH + CH₂), 6.37 (s, 2H, CH_{Ar}), 6.48 (s, 1H, CH_{Naph}), 6.70 (s, 1H, CH_{Naph}), 9.74 (s, 1H, NH); ¹³C NMR (DMSO-*d*₆) δ 23.2 (CH₂), 28.7 (CH₂), 28.9 (CH), 56.3 (OCH₃), 60.3 (OCH₃), 65.5 (OCH₂), 95.1 (C=C–NH), 105.3 (C_{Ar}), 116.4 (C_{Ar}), 122.3 (C_{Ar}), 131.1 (C_{Ar}), 131.9 (C_{Ar}), 132.0 (C_{Ar}), 134.0 (C_{Ar}), 136.3 (C_{Ar}), 136.4 (C_{Ar}), 143.4 (C_{Ar}), 153.2 (C_{Ar}), 153.3 (C_{Ar}), 159.1 (C_{Ar}), 172.8 (C=O); HRMS m/z (ESI) calcd for $C_{24}H_{25}NO_5Na$ ($M + Na$)⁺ 430.1630, found 430.1626.

11-(3,5-Dibromophenyl)-4,6,7,8,9,11-hexahydrobenzo[g]furo[3,4-b]quinolin-1(3H)-one (41). 31% yield as white solid, mp ≥ 300 °C (CHCl₃/MeOH = 20/1). ¹H NMR (DMSO-*d*₆) δ 1.62 (s, 4H), 2.50 (s, 4H), 4.83–5.00 (dd, *J* = 15 Hz, 2H), 4.99 (s, 1H), 6.62 (s, 1H), 6.69 (s, 1H), 7.38 (s, 2H), 7.61 (s, 1H), 10.05 (s, 1H); ¹³C NMR (DMSO-*d*₆) δ 23.1, 23.2, 28.7, 29.0, 65.8, 94.3, 116.8, 121.1, 123.1, 130.3, 131.3, 131.9, 132.5, 134.1, 137.1, 151.9, 159.5, 172.5; HRMS m/z (ESI) calcd for $C_{21}H_{13}Br_2NO_3Na$ ($M + Na$)⁺ 495.9524, found 495.9519.

6-(3,4,5-Trimethoxyphenyl)-3,6,9,10-tetrahydro-7H-furo[3,4-b]pyrrolo[2,3-h]quinolin-7-one (42). 56% yield as brown solid, mp ≥ 300 °C (CHCl₃/MeOH = 20/1). ¹H NMR (DMSO-*d*₆) δ 3.60 (s, 3H, OCH₃), 3.69 (s, 6H, OCH₃), 4.93–5.09 (dd, *J* = 15 Hz, 2H, CH₂), 5.05 (s, 1H, CH), 6.52 (s, 2H, CH_{Ar}), 6.66 (s, 1H, H_{α-Ind}), 6.84 (d, *J* = 6.0 Hz, 1H, CH_{Ind-7}), 7.00 (d, *J* = 6.0 Hz, 1H, CH_{Ind-6}), 7.31 (t, *J* = 3.0 Hz, 1H, H_{β-Ind}), 9.99 (s, 1H, NH), 11.15 (s, 1H, NH); ¹³C NMR (DMSO-*d*₆) δ 55.8 (OCH₃), 59.8 (OCH₃), 65.2 (OCH₂), 95.6 (C_{Ar}), 98.2 (C_{Ar}), 105.1 (C_{Ar}), 107.0 (C_{Ar}), 112.7 (C_{Ar}), 116.9 (C_{Ar}), 123.7 (C_{Ar}), 124.7 (C_{Ar}), 127.6 (C_{Ar}), 135.8 (C_{Ar}), 143.5 (C_{Ar}), 152.6 (C_{Ar}), 158.4 (C_{Ar}), 172.4 (C=O); HRMS m/z (ESI) calcd for $C_{22}H_{20}N_2O_5K$ ($M + K$)⁺ 431.1009, found 431.1005.

6-(3,5-Dibromophenyl)-3,6,9,10-tetrahydro-7H-furo[3,4-b]pyrrolo[2,3-h]quinolin-7-one (43). 39% yield as brown solid, mp ≥ 300 °C (CHCl₃/MeOH = 20/1). ¹H NMR (DMSO-*d*₆) δ 4.96–5.17 (m, 3H), 6.67 (s, 2H), 7.01 (s, 1H), 7.32–7.59 (m, 4H), 10.09 (s, 1H), 11.25 (s, 1H); ¹³C NMR (DMSO-*d*₆) δ 66.0, 95.4, 98.8, 108.1, 112.0, 117.7, 123.0, 124.2, 125.7, 128.4, 130.4, 131.7, 136.2, 152.6, 159.4, 172.8; HRMS m/z (ESI) calcd for $C_{19}H_{12}Br_2N_2O_2Na$ ($M + Na$)⁺ 480.9163, found 480.9164.

4-(3,4,5-Trimethoxyphenyl)-4,8-dihydro-1H-furo[3,4-b]pyrazolo[4,3-e]pyridine-3,5(2H,7H)-dione (44). 45% yield as pink solid, mp = 186–188 °C (CHCl₃/MeOH = 20/1). ¹H NMR (DMSO-*d*₆) δ 3.69 (s, 3H, OCH₃), 3.71 (s, 6H, OCH₃), 4.33–4.57 (m, 3H, CH+CH₂), 6.61 (s, 1H, CH_{Ar}), 6.77 (s, 1H, CH_{Ar}); ¹³C NMR (DMSO-*d*₆) δ 33.4 (CH), 56.3 (OCH₃), 60.5 (OCH₃), 68.3 (OCH₃), 89.2 (C_{Ar}), 104.8 (C_{Ar}), 105.3 (C_{Ar}), 136.3 (C_{Ar}), 142.2 (C_{Ar}), 152.9 (C_{Ar}), 155.9 (C_{Ar}), 177.5 (C=O), 181.5 (C=O); HRMS m/z (ESI) calcd for $C_{17}H_{16}N_3O_6$ ($M + H$)⁺ 358.1039, found 358.1030.

4-(3,5-Dibromophenyl)-4,8-dihydro-1H-furo[3,4-*b*]pyrazolo[4,3-*e*]pyridine-3,5(2*H*,7*H*)-dione (45). 38% yield as orange solid, mp = 228–230 °C (CHCl₃/MeOH = 20/1). ¹H NMR (DMSO-*d*₆) δ 4.31–4.46 (dd, *J* = 15 Hz, 2H), 5.35 (s, 3H), 7.35 (s, 1H), 7.81 (s, 2H), 7.97 (s, 1H); ¹³C NMR (DMSO-*d*₆) δ 68.4, 69.2, 97.2, 104.1, 108.7, 121.7, 122.7, 129.1, 132.6, 134.5, 135.0, 155.0, 155.9, 168.6, 177.1, 181.9; HRMS *m/z* (ESI) calcd for C₁₄H₁₀Br₂N₃O₃ (M + H)⁺ 425.9089, found 425.9089.

4-Amino-2-(methylsulfanyl)-5-(3,4,5-trimethoxyphenyl)-5,9-dihydrofuro[3',4':5,6]pyrido[2,3-*d*]pyrimidin-6(8*H*)-one (46). 60% yield as white solid, mp = 261–262 °C, dec (CHCl₃/MeOH = 20/1). ¹H NMR (DMSO-*d*₆) δ 2.35 (s, 3H, SCH₃), 3.59 (s, 3H, OCH₃), 3.69 (s, 6H, OCH₃), 3.99–4.27 (m, 3H, CH + CH₂), 5.96 (s, 1H, NH), 6.11 (s, 1H, NH), 6.66 (s, 2H, CH_{Ar}), 7.55 (s, 1H, NH); ¹³C NMR (DMSO-*d*₆) δ 13.5 (SCH₃), 35.5 (CH), 50.7(OCH₂), 56.4 (OCH₃), 60.4 (OCH₃), 74.7 (C_{Ar}), 83.0 (C_{Ar}), 86.5 (C_{Ar}), 106.6 (C_{Ar}), 136.6 (C_{Ar}), 137.5 (C_{Ar}), 152.9 (C_{Ar}), 157.7 (C_{Ar}), 161. (C_{Ar})₁, 167.9 (C_{Ar})₁, 175.2 (C=O); HRMS *m/z* (ESI) calcd for C₁₉H₂₀N₄O₅Na (M + Na)⁺ 439.1052, found 439.1062.

4-Amino-5-(3,5-dibromophenyl)-2-(methylsulfanyl)-5,9-dihydrofuro[3',4':5,6]pyrido [2,3-*d*]pyrimidin-6(8*H*)-one (47). 36% yield as white solid, mp = 205–207 °C (CHCl₃/MeOH = 20/1). ¹H NMR (DMSO-*d*₆) δ 2.34 (s, 3H), 4.77–4.92 (dd, *J* = 8.0 Hz, 2H), 5.39 (s, 1H), 7.44 (m, 2H), 7.66–7.77 (m, 2H), 8.07 (s, 1H), 10.41 (s, 1H); ¹³C NMR (DMSO-*d*₆) δ 13.7, 33.9, 66.0, 69.7, 90.8, 99.0, 123.4, 131.0, 135.4, 148.6, 154.8, 162.6, 168.0, 175.5; HRMS *m/z* (ESI) calcd for C₁₆H₁₃Br₂N₄O₂S (M + H)⁺ 482.9126, found 482.9128.

Cell Culture. Human T-cell leukemia cell line Jurkat (ATCC TIB-152, E6-1 clone) was cultured in RPMI-1640 (Invitrogen) supplemented with 10% FBS (Invitrogen), 100 mg/L penicillin G, 100 mg/L streptomycin, 1.0 mM sodium pyruvate, 1.5 g/L sodium bicarbonate, and 4.5 g/L glucose (all from Sigma). Human cervical cancer cell line HeLa (ATCC S3) was cultured in DMEM (Invitrogen) supplemented with 10% FBS, 100 mg/L penicillin G, and 100 mg/L streptomycin. MCF-7 (human mammary carcinoma) cells were cultured in DMEM supplemented with 1.0 mM sodium pyruvate, 1% GlutaMax-1 (Invitrogen), 100 μg/mL penicillin, 100 μg/mL streptomycin, and 10% FBS. The cells were incubated at 37 °C in a humidified atmosphere with 5% CO₂.

MTT Assay. An amount of 100 μL of HeLa or MCF-7 cells was transferred to each well of a 96-well microtiter plate at 2 × 10⁴ cells/mL and incubated for 24 h to allow proper adhesion. Cells were treated with the panel of test compounds at a series of concentrations and DMSO as control. After 48 h of incubation, 20 μL of MTT reagent (5 mg/mL) was added to each well of the plates. The plate was incubated for 2 h at 37 °C. The media were removed from each well of the plate, and the resulting formazan crystals were dissolved in 100 μL of DMSO. Optical density (OD) at 490 nm was measured using a ThermoMAX microplate reader. The experiments were performed in eight replicates and repeated at least twice for each compound per cell line.

Annexin-V Apoptosis Assay. An amount of 2 × 10⁵ Jurkat cells/mL was plated in 24-well plates, treated with the test compounds at a range of concentrations, and incubated for 48 h. The cells were centrifuged at 400g for 1 min. The supernatant was discarded, and the cells were resuspended in 100 μL per sample of annexin-V-FITC/propidium iodide solution in HHB (3 μL of CaCl₂ (1.5 M) per mL of HHB, 2 μL (10 mg/mL) of propidium iodide (Sigma) per mL of HHB, and 20 μL of annexin-V-FITC (Southern Biotech) per mL of HHB). The samples in the labeling solution were transferred into Falcon tubes and incubated in a water bath at 37 °C for 20 min. The samples were then analyzed using a Becton Dickinson FACScan flow cytometer with CellQuest software. The results were tabulated as % of annexin-V-FITC positive apoptotic cells. The experiments were performed in three replicates and repeated at least twice for each compound.

Caspase-3 Activity Assay. Caspase-3 activation was detected by using a caspase-3 colorimetric activity assay kit (Chemicon), which assays the activity of caspase-3, recognizing the sequence DEVD. The assay is based on spectrophotometric detection of *p*-nitroaniline (pNA) after cleavage of the labeled substrate DVED-*p*-NA. Therefore, Jurkat cells were treated with a panel of test compounds (0.1, 0.5, and 1 μM), DMSO, and podophyllotoxin (0.1, 0.5, and 1 μM). 1 × 10⁶ cells were harvested and lysed with lysis buffer. Protein concentration of each sample was determined using Pierce BCA protein assay kit (Pierce). Each sample was mixed with caspase-3 substrate (DEVD-*p*-nitroaniline) and incubated at 37 °C for 2 h in 96-well plates (LPS). Samples were read at 405 nm using a spectrophotometer (Molecular Devices). The experiments were performed in quadruplicate and repeated at least twice for each compound.

In Vitro Tubulin Polymerization Assay. The in vitro tubulin polymerization assay was conducted as described by the manufacturer (Cytoskeleton Inc.). In brief, paclitaxel, DMSO, **10**, **16**, and podophyllotoxin were incubated with purified bovine tubulin and buffer containing 10% glycerol and 1 mM GTP at 37 °C each in a separate experiment. The effect of each agent on tubulin polymerization was monitored in a temperature-controlled Carey Eclipse fluorescence spectrophotometer (Varian) for 20 min, with readings acquired every 15 s.

Morphological Analysis of Microtubule Organization in HeLa Cells. HeLa cells were cultured in DMEM supplemented with 10% fetal calf serum, sodium pyruvate, sodium bicarbonate, and PSF. For dihydropyridopyrazole treatments, cells were treated for 3 h with either carrier (0.1% DMSO) or compounds solubilized in DMSO and prediluted in media prior to fixation by immersion in methanol at –20 °C. Cells were subsequently rehydrated in phosphate-buffered saline (PBS) and blocked by incubation in PBS containing 5% bovine serum albumin for 1 h at 20 °C. Cells were then incubated with Hoechst 33342 (Molecular Probes), mouse anti-tubulin (Sigma), and rabbit anti-Hec1 (Abcam) in PBS-BSA overnight at 4 °C. Primary antibodies were detected using Alexafluor-conjugated secondary antibodies (Molecular Probes), and images were acquired using a Zeiss Axiovert 200M inverted microscope equipped with epifluorescence optics and an Apotome structured illumination module (Carl Zeiss). All acquired images were exported into eight bit tiff files, and figures were prepared using Adobe Photoshop software.

■ ASSOCIATED CONTENT

Supporting Information. Details of DFT optimization and docking procedures, an enlarged version of Figure 4, details of chiral HPLC, ¹H and ¹³C NMR spectra of all new compounds, and crystallography data in CIF format. This material is available free of charge via the Internet at <http://pubs.acs.org>.

■ AUTHOR INFORMATION

Corresponding Author

*For I.V.M.: phone, +1 575 835 6886; fax, +1 575 835 5364; e-mail, imagedov@nmt.edu. For W.A.L.v.O.: phone, +27 21 808 3344; fax, +27 21 808 3360; e-mail, wvo@sun.ac.za. For A.K.: phone, +1 575 835 5884; fax, +1 575 835 5364; e-mail, akornien@nmt.edu.

Present Addresses

•School of Science, Technology and Engineering Management, St. Thomas University, 16401 NW 37th Avenue, Miami Gardens, FL 33054, United States.

■ ACKNOWLEDGMENT

This work is supported by the U.S. National Institutes of Health (Grants RR-16480 and CA-135579) under the BRIN/INBRE

and AREA programs. W.A.L.v.O. gratefully acknowledges funding from the Research Office, University of the Witwatersrand, South Africa, for supporting this collaboration (postdoctoral fellowship to U.d.B.), the National Research Foundation (NRF, Pretoria, South Africa) for research funding and the Alexander van Humboldt Foundation for a Georg-Forster Experienced Researcher fellowship with Profs. Herbert Waldmann and Daniel Rauh at the MPI and Technical University Dortmund, Germany. We thank Mr. H. Dücker and Ms. N. Martinez (MPI-Dortmund) for assistance with the chiral-prep HPLC and the Mass Spectrometry Facility at the University of New Mexico for HRMS data.

ABBREVIATIONS USED

ATCC, American Type Culture Collection; DMEM, Dulbecco's modified Eagle's medium; DFT, density functional theory; DMF, dimethylformamide; DMSO, dimethylsulfoxide; ECACC, European Collection of Cell Culture; EDTA, diethylenetriaminepentaacetic acid; EtOH, ethanol; FBS, fetal bovine serum; FITC, fluorescein isothiocyanate; HEPES, 4-(2-hydroxyethyl)-1-piperazineethanesulfonic acid; HHB, Heinz HEPES buffer; HRMS, high resolution mass spectrometry; MCR, multicomponent reaction; MTT, 3-(4,5-dimethylthiazol-2-yl)-2,5-diphenyltetrazolium bromide; PDB, Protein Data Bank; RU, relative units; SAR, structure-activity relationship; TLC, thin layer chromatography; SD, standard deviation

REFERENCES

- (1) Koehn, F. E.; Carter, G. T. The evolving role of natural products in drug discovery. *Nat. Rev. Drug Discovery* **2005**, *4*, 206–220.
- (2) Newman, D. J.; Cragg, G. M.; Snader, K. M. Natural products as sources of new drugs over the period 1981–2002. *J. Nat. Prod.* **2003**, *66*, 1022–1037.
- (3) Breinbauer, R.; Vetter, I. R.; Waldmann, H. From protein domains to drug candidates—natural products as guiding principles in the design and synthesis of compound libraries. *Angew. Chem., Int. Ed.* **2002**, *41*, 2879–2890.
- (4) Harvey, A. L. Natural products in drug discovery. *Drug Discovery Today* **2008**, *13*, 894–901.
- (5) (a) Magedov, I. V.; Manpadi, M.; Rozhkova, E.; Przheval'skii, N. M.; Rogelj, S.; Shors, S. T.; Steelant, W. F. A.; Van Slambrouck, S.; Kornienko, A. Structural simplification of bioactive natural products with multicomponent synthesis: dihydropyridopyrazole analogues of podophyllotoxin. *Bioorg. Med. Chem. Lett.* **2007**, *17*, 1381–1385. (b) Magedov, I. V.; Manpadi, M.; Van Slambrouck, S.; Steelant, W. F. A.; Rozhkova, E.; Przheval'skii, N. M.; Rogelj, S.; Kornienko, A. Discovery and investigation of antiproliferative and apoptosis-inducing properties of new heterocyclic podophyllotoxin analogues accessible by a one-step multicomponent synthesis. *J. Med. Chem.* **2007**, *50*, 5183–5192. (c) Magedov, I. V.; Manpadi, M.; Evdokimov, N. M.; Elias, E. M.; Rozhkova, E.; Ogasawara, M. A.; Bettale, J. D.; Przeval'skii, N. M.; Rogelj, S.; Kornienko, A. Antiproliferative and apoptosis inducing properties of pyrano[3,2-*c*]pyridones accessible by a one-step multicomponent synthesis. *Bioorg. Med. Chem. Lett.* **2007**, *17*, 3872–3876. (d) Magedov, I. V.; Manpadi, M.; Ogasawara, M. A.; Dhawan, A. S.; Rogelj, S.; Van Slambrouck, S.; Steelant, W. F. A.; Evdokimov, N. M.; Uginskii, P. Y.; Elias, E. M.; Knee, E. J.; Tongwa, P.; Antipin, M. Y.; Kornienko, A. Structural simplification of bioactive natural products with multicomponent synthesis. 2. Antiproliferative and antitubulin activities of pyrano[3,2-*c*]pyridones and pyrano[3,2-*c*]quinolones. *J. Med. Chem.* **2008**, *51*, 2561–2570. (e) Evdokimov, N. M.; Van Slambrouck, S.; Heffeter, P.; Tu, L.; Le Calve, B.; Lamoral-Theys, D.; Hooten, C. J.; Uginskii, P. Y.; Rogelj, S.; Kiss, R.; Steelant, W. F. A.; Berger, W.; Bologna, C. J.; Yang, J. J.; Kornienko, A.; Magedov, I. V. Structural simplification of bioactive natural products with multicomponent synthesis. 3. Fused uracil-containing heterocycles as novel topoisomerase-targeting agents. *J. Med. Chem.* **2011**, *54*, 2012–2021.
- (6) Bohlin, L.; Rosen, B. Podophyllotoxin derivatives: drug discovery and development. *Drug Discovery Today* **1996**, *1*, 343–351.
- (7) For reviews, see the following: (a) You, Y. J. Podophyllotoxin derivatives: current synthetic approaches for new anticancer agents. *Curr. Pharm. Des.* **2005**, *11*, 1695–1717. (b) Gordaliza, M.; Castro, M. A.; Corral, J. M. M.; San Feliciano, A. Antitumor properties of podophyllotoxin and related compounds. *Curr. Pharm. Des.* **2000**, *6*, 1811–1839.
- (8) Berkowitz, D. B.; Maeng, J.-H.; Dantzig, A. H.; Shepard, R. L.; Norman, B. H. Chemoenzymatic and ring E-modular approach to the (–)-podophyllotoxin skeleton. Synthesis of 3',4',5'-tridemethoxy(–)-podophyllotoxin. *J. Am. Chem. Soc.* **1996**, *118*, 9426–9427.
- (9) See for example: Vial, J. P.; Belloc, F.; Dumain, P.; Besnard, S.; Lacombe, F.; Boisseau, M. R.; Reiffers, J.; Bernard, P. Study of the apoptosis induced in vitro by antitumoral drugs on leukaemic cells. *Leuk. Res.* **1997**, *21*, 163–172.
- (10) Kemnitzer, W.; Drewe, J.; Jiang, S.; Zhang, H.; Wang, Y.; Zhao, J.; Jia, S.; Herich, J.; Labreque, D.; Storer, R.; Meerovitch, K.; Bouffard, D.; Rej, R.; Denis, R.; Blais, C.; Lamothe, S.; Attardo, G.; Gourdeau, H.; Tseng, B.; Kasibhatla, S.; Cai, S. X. Discovery of 4-aryl-4*H*-chromenes as a new series of apoptosis inducers using a cell- and caspase-based high-throughput screening assay. 1. Structure-activity relationships of the 4-aryl group. *J. Med. Chem.* **2004**, *47*, 6299–6310.
- (11) (a) Vermes, I.; Haanen, C.; Steffens-Nakken, H.; Reutelingsperger, C. A novel assay for apoptosis—flow cytometric detection of phosphatidylserine expression on early apoptotic cells using fluorescein-labeled annexin-V. *Immunol. Methods* **1995**, *184*, 39–51. (b) Fadok, V. A.; Voelker, D. R.; Campbell, P. A.; Cohen, J. J.; Bratton, D. L.; Henson, P. M. Exposure of phosphatidylserine on the surface of apoptotic lymphocytes triggers specific recognition and removal by macrophages. *J. Immunol.* **1992**, *148*, 2207–2216.
- (12) Kasibhatla, S.; Gourdeau, H.; Meerovitch, K.; Drewe, J.; Reddy, S.; Qiu, L.; Zhang, H.; Bergeron, F.; Bouffard, D.; Yang, Q.; Herich, J.; Lamothe, S.; Cai, S. X.; Tseng, B. Discovery and mechanism of action of a novel series of apoptosis inducers with potential vascular targeting activity. *Mol. Cancer Ther.* **2004**, *3*, 1365–1373.
- (13) Hamel, E. Evaluation of antimetabolic agents by quantitative comparisons of their effects on the polymerization of purified tubulin. *Cell Biochem. Biophys.* **2003**, *38*, 1–21.
- (14) (a) Frackepohl, J.; Adelt, I.; Antonicek, H.; Arnold, C.; Behrmann, P.; Blaha, N.; Bohmer, J.; Gutbrod, O.; Hanke, R.; Hohmann, S.; van Houtdrevre, M.; Losel, P.; Malsam, O.; Melchers, M.; Neufert, V.; Peschel, E.; Reckmann, U.; Schenke, T.; Thiesen, H. P.; Velten, R.; Vogelsang, K.; Weiss, H. C. Insecticidal heterolignans-tubuline polymerization inhibitors with activity against chewing pests. *Bioorg. Med. Chem.* **2009**, *17*, 4160–4184. (b) For the first study of the utilization of anilines in this MCR, see the following: Tratrat, C.; Giorgi-Renault, S.; Husson, H. P. A multicomponent reaction for the one-pot synthesis of 4-aza-2,3-didehydropodophyllotoxin and derivatives. *Org. Lett.* **2002**, *4*, 3187–3189.
- (15) (a) Tu, S.; Zhang, Y.; Zhang, J.; Jiang, B.; Jia, R.; Zhang, J.; Ji, S. A simple procedure for the synthesis of 4-aza-podophyllotoxin derivatives in water under microwave irradiation conditions. *Synlett* **2006**, 2785–2790. (b) Kozlov, N. G.; Bondarev, S. L.; Kadutskii, A. P.; Basalava, L. I.; Pashkovskii, F. S. Tetric acid in reaction with aromatic aldehydes and 2-naphthylamine. Investigation of fluorescent and nonlinear-optical characteristics of compounds obtained. *Russ. J. Org. Chem.* **2008**, *44*, 1031–1037.
- (16) (a) Khurana, J. M.; Magoo, D. pTSA-catalyzed one-pot synthesis of 12-aryl-8,9,10,12-tetrahydrobenzo[*a*]xanthen-11-ones in ionic liquid and neat conditions. *Tetrahedron Lett.* **2009**, *50*, 4777–4780. (b) Wang, R. Z.; Zhang, L. F.; Cui, Z. S. Iodine-catalyzed synthesis of 12-aryl-8,9,10,12-tetrahydro-benzo[*a*]xanthen-11-one derivatives via multicomponent reaction. *Synth. Commun.* **2009**, *39*, 2101–2107. (c) Gao, S.; Tsai, C. H.; Yao, C. F. A simple and green approach for the synthesis of tetrahydrobenzo[*a*]xanthen-11-one derivatives using tetrabutyl ammonium fluoride in water. *Synlett* **2009**, 949–954. (d) Nandi, G. C.;

Samai, S.; Kumar, R.; Singh, M. S. An efficient one-pot synthesis of tetrahydrobenzo[*a*]xanthene-11-one and diazabenzo[*a*]anthracene-9,11-dione derivatives under solvent free condition. *Tetrahedron* **2009**, *65*, 7129–7134. (e) Li, J.; Tang, W.; Lu, L.; Su, W. Strontium triflate catalyzed one-pot condensation of beta-naphthol, aldehydes and cyclic 1,3-dicarbonyl compounds. *Tetrahedron Lett.* **2008**, *49*, 7117–7120. (f) Das, B.; Laxminarayana, K.; Krishnaiah, M.; Srinivas, Y. An efficient and convenient protocol for the synthesis of novel 12-aryl- or 12-alkyl-8,9,10,12-tetrahydrobenzo[*a*]xanthen-11-one derivatives. *Synlett* **2007**, 3107–3112.

(17) These results will be published elsewhere.

(18) Brewer, C. F.; Loike, J. D.; Horwitz, S. B. Conformational-analysis of podophyllotoxin and its congeners. Structure–activity relationships in microtubule assembly. *J. Med. Chem.* **1979**, *22*, 215–221.

(19) Ravelli, R. B. G.; Gigant, B.; Curmi, P. A.; Jourdain, I.; Lachkar, S.; Sobel, A.; Knossow, M. Insight into tubulin regulation from a complex with colchicine and a stathmin-like domain. *Nature* **2004**, *428*, 198–202.

(20) (a) Alam, A.; Naik, P. K. Molecular modelling evaluation of the cytotoxic activity of podophyllotoxin analogues. *J. Comput.-Aided Mol. Des.* **2009**, *23*, 209–225. (b) Verma, R. P.; Hansch, C. A QSAR study on the cytotoxicity of podophyllotoxin analogues against various cancer cell lines. *Med. Chem.* **2010**, *6*, 79–86. (c) Villanueva, H. E.; Setzer, W. N. Cembrene diterpenoids: conformational studies and molecular docking to tubulin. *Rec. Nat. Prod.* **2010**, *4*, 115–123.

(21) Kim do, Y.; Kim, K. H.; Kim, N. D.; Lee, K. Y.; Han, C. K.; Yoon, J. H.; Moon, S. K.; Lee, S. S.; Seong, B. L. Design and biological evaluation of novel tubulin inhibitors as antimetabolic agents using pharmacophore binding model with tubulin. *J. Med. Chem.* **2006**, *49*, 5664–5670.